

---

# ITERATIVE BARYCENTER FLOWS

---

A PREPRINT

**David I. Inouye**  
Purdue University  
dinouye@purdue.edu

**Zeyu Zhou**  
Purdue University  
zhou1059@purdue.edu

**Ziyu Gong**  
Purdue University  
gong123@purdue.edu

**Pradeep Ravikumar**  
Carnegie Mellon University  
pradeepr@cs.cmu.edu

April 16, 2021

## ABSTRACT

The task of mapping two or more distributions to a shared representation has many applications including fair representations, batch effect mitigation, and unsupervised domain adaptation. However, most existing formulations only consider the setting of two distributions, and moreover, do not have an identifiable, unique shared latent representation. We use optimal transport theory to consider a natural multiple distribution extension of the Monge assignment problem we call the symmetric Monge map problem and show that it is equivalent to the Wasserstein barycenter problem. Yet, the maps to the barycenter are challenging to estimate. Prior methods often ignore transportation cost, rely on adversarial methods, or only work for discrete distributions. Therefore, our goal is to estimate invertible maps between two or more distributions and their corresponding barycenter via a simple iterative flow method. Our method decouples each iteration into two subproblems: 1) estimate simple distributions and 2) estimate the invertible maps to the barycenter via known closed-form OT results. Our empirical results give evidence that this iterative algorithm approximates the maps to the barycenter.

## 1 INTRODUCTION

The task of mapping two or more distributions to a shared representation has attracted increasing interest due to its varied applications. These include fair representations [Zemel et al., 2013], batch effect mitigation [Haghverdi et al., 2018], unsupervised domain adaptation [Hu et al., 2018], and generative models [Grover et al., 2020]. For example, Zemel et al. [2013] estimate a shared latent representation of the class-conditional distributions that simultaneously obfuscates any information about protected attributes (e.g., race) while preserving all other information useful for classification. For genetic data, Haghverdi et al. [2018] attempt to mitigate batch effects (i.e., irrelevant shifts in the data between batches caused by non-biological factors) by estimating a shared representation among batches; this enables the integration and analysis of multiple datasets collected at different laboratories. Hu et al. [2018] perform unsupervised domain adaptation by mapping the source and target domains to a shared latent representation. In most existing formulations for this task (of finding mappings from multiple distributions to a shared representation) however, the mapping to the shared representation and sometimes even the shared representation itself is under constrained and non-unique (e.g., [Grover et al., 2020]). This lack of identifiability of course has algorithmic implications (such as possible oscillatory non-convergent behavior), but moreover also poses theoretical concerns (since the target of the estimation procedures is unclear). While it might be possible to impose constraints on the mappings to ensure identifiability, it is not clear what such natural constraints might be.

In this paper, we propose to use the theory of optimal transport (OT) towards the task of *identifiable mappings* from multiple distributions to a shared representation: by adding the additional restriction of requiring the mappings to have the *least transportation cost*. This can be shown to provide a natural and importantly — unique — shared latent representation. Moreover, as we show in the experiments, the resulting shared latent representations are much more meaningful: because they aim to minimize transportation cost, the maps are parsimonious in transforming each distribution, and in particular, preserve shared structure among the different distributions. For instance, the shared representation among digits should be digit-like. Whereas, methods ignore transportation cost, typically transform the class distributions to some baseline distribution such as uniform or Gaussian. We believe that such un-parsimonious

transformations would accordingly incur greater sample complexity; this is particularly so if the distributions are approximately singular and lie on a lower dimensional manifold (e.g., images of digits).

Recall the classical Monge assignment problem which aims to find the mapping from one distribution to another with the least cost. One (minor) caveat with this formulation is that this is not a symmetric formulation, but more importantly, this is focused on the case of two distributions. We thus consider a natural multiple distribution symmetric extension of the Monge assignment problem, which we call the symmetric Monge map problem: where we aim to find mappings from multiple distributions to a shared latent distribution, but with the least transport costs. Interestingly, under some regularity conditions, this turns out to be equivalent to the *barycenter* of the given distributions, which can be seen as an extension of the Euclidean mean to distributions [Peyré and Cuturi, 2019]. From OT theory, we have that the optimal map from each of the distributions to this barycenter for continuous distributions is unique and invertible. Thus, OT theory identifies a principled and theoretically-grounded shared representation with unique corresponding maps.

There is however a critical computational caveat with the formulation above: barycenter distributions and OT maps are challenging to estimate, especially given only samples. Most prior practical barycenter work has focused on estimating barycenters in discrete spaces (see e.g., [Peyré and Cuturi, 2019]). While the continuous problem can be approximated by discretizing the space via histograms or clustering, this approach will fail in higher dimensions because of the curse of dimensionality. Another approach is to solve the barycenter problem directly on samples and then use a neural network to interpolate for new data points [Seguy et al., 2018], but this process only learns the map indirectly and does not guarantee invertibility. Thus, in spite of the theoretical advantage of identifiability and the parsimony of shared representations, simply using existing Barycenter algorithms might be less scalable than the non-OT deep generative approaches that are popularly used for this task. In particular, flow-based deep generative methods learn invertible mappings between distributions by construction (e.g., [Dinh et al., 2017, Kingma et al., 2016, Kingma and Dhariwal, 2018]), but these methods do not learn an identifiable mapping, ignore transportation costs (e.g., [Dinh et al., 2017]), and moreover, might require adversarial methods (e.g., [Grover et al., 2020]), which can be difficult to optimize in practice [Lucic et al., 2018, Kurach et al., 2019].

We thus aim to develop a simple class of scalable iterative algorithms for approximating the maps to the shared barycenter distribution. Instead of trying to solve the global problem directly, we propose to iteratively solve simpler subproblems by first approximating the class distributions and then estimating the barycenter maps by leveraging known closed-form results (particularly for Gaussians and 1D problems). This can be seen as optimizing approximate subproblems rather than approximately solving a large joint problem—similar in spirit to Newton’s method or coordinate descent. We summarize our contributions as follows:

- We formulate the problem of estimating the maps from multiple distributions to a shared latent representation as a symmetric Monge map problem whose solution is unique; we show that it is equivalent to the barycenter problem and uncover its relationship to prior adversarial and flow-based methods.
- We propose a general iterative meta-algorithm to approximately optimize this symmetric Monge map problem via iteratively solving two steps: given respective samples, estimate distributions from simple parametric families, estimate the symmetric Monge map problem for these estimated distributions via known closed-form results, and then using the Monge maps to transform the respective samples for the next iteration.
- We provide three concrete instantiations of the above general meta-algorithm and demonstrate that our approach approximates the mappings to the barycenter on several simulated and real-world datasets.

## 2 SYMMETRIC MONGE MAPS

### 2.1 Background: Classical Monge Maps

We will first review some standard OT definitions. First, we note that  $T_{\sharp}\alpha$  will denote the push-forward measure of  $\alpha$  via the map  $T$  (see [Peyré and Cuturi, 2019, Def. 2.1]).

**Definition 1** (Monge problem [Peyré and Cuturi, 2019, Remark 2.7]). *Given two measures  $(\alpha, \beta)$  supported on two spaces  $(\mathcal{X}, \mathcal{Y})$  and a cost function  $c(\cdot, \cdot)$ , the Monge problem is defined as finding the map  $T: \mathcal{X} \rightarrow \mathcal{Y}$  that solves:*

$$\arg \min_T \int_{\mathcal{X}} c(x, T(x)) d\alpha(x) \quad \text{s.t.} \quad T_{\sharp}\alpha = \beta.$$

We will denote the optimal Monge map between two distributions as  $T_{\alpha \rightarrow \beta}^*$  where  $\alpha$  and  $\beta$  represent two distributions.

## 2.2 Symmetric Monge Map Formulation

We note that the Monge formulation is asymmetric because the two distributions have distinct roles. While in theory the role of the distributions does not matter because  $T_{2 \rightarrow 1}^* \equiv (T_{1 \rightarrow 2}^*)^{-1}$ , in practice the estimated map  $\hat{T}$  will vary depending on which distribution is the source distribution. Finally and more importantly, the Monge problem in its original formulation only considers two distributions but we want to consider more than two distributions.

**Definition 2** (Symmetric Monge Map). *Given a set of continuous input measures  $(\mu_1, \dots, \mu_k)$  defined on some continuous space  $\mathcal{X}$ , a non-negative weight vector  $w \geq 0$  such that  $\sum_j w_j = 1$ , and cost function  $c(\cdot, \cdot)$ , the symmetric Monge map problem is defined as:*

$$\arg \min_{T_1, T_2, \dots, T_k} \sum_{j=1}^k w_j \int_{\mathcal{X}} c(x, T_j(x)) d\mu_j(x) \quad (1)$$

$$\text{s.t. } T_{j\#} \mu_j = T_{j'\#} \mu_{j'} \quad \forall j \neq j', \quad (2)$$

where Eqn. 1 is the transportation cost and Eqn. 2 is known as the pushforward condition.

The original Monge problem can be recovered if  $T_2 = \text{id}$  and  $w_2 = 0$ . Thus, this problem can be seen as a symmetric relaxation of the Monge problem for two or more distributions. The pushforward condition in Eqn. 2 is hard to satisfy for continuous distributions known only through samples.

## 2.3 Equivalence to Barycenter

We prove that our symmetric Monge map problem is equivalent to the barycenter problem (proof in appendix). We first review the definitions of the Kantorovich relaxation and the barycenter distribution, and then present our theorem. For this paper, we will assume  $c(x, y) = \|x - y\|_2^2$  and that one of the measures has a density so that the barycenter is unique [Agué and Carlier, 2011].

**Definition 3** (Kantorovich Relaxation [Peyré and Cuturi, 2019, Remark 2.13]). *Given the same variables as Def. 1, the Kantorovich problem is defined as:  $\mathcal{L}_c(\alpha, \beta) \triangleq \min_{\pi \in \mathcal{U}(\alpha, \beta)} \int_{\mathcal{X} \times \mathcal{Y}} c(x, y) d\pi(x, y)$ , where  $\pi$  is a joint distribution over  $\mathcal{X}$  and  $\mathcal{Y}$  such that the marginals are equal to  $\alpha$  and  $\beta$  respectively (denoted by  $\mathcal{U}(\alpha, \beta)$ ).*

**Definition 4** (Wasserstein Barycenter [Peyré and Cuturi, 2019, Remark 9.1]). *Given a set of input measures  $(\mu_1, \dots, \mu_k)$  defined on some space  $\mathcal{X}$ , weights  $w$  such that  $\sum_j w_j = 1$ , the barycenter is defined as:  $\text{bary}(\mu_1, \mu_2, \dots, \mu_k; w) \triangleq \arg \min_{\nu} \sum_{j=1}^k w_j \mathcal{L}_c(\nu, \mu_j)$ , where  $\mathcal{L}_c$  is defined in Def. 3.*

**Theorem 1** (Barycenter Equivalence for Symmetric Monge Map). *For  $c(x, y) = \|x - y\|_2^2$  where the measures have densities, the symmetric Monge map solution (Def. 2) gives the optimal maps between the class distributions and the barycenter distribution (Def. 4), i.e.,  $T_j^* = T_{j \rightarrow \nu}^*$  where  $\nu = \text{bary}(\mu_1, \mu_2, \dots, \mu_k; w)$ .*

## 2.4 Relation to Prior Methods

**Adversarial Methods** CycleGAN [Zhu et al., 2017] minimizes the fairly complex objective function:

$$\arg \min_{G, F} d_{\text{adv}}(G_{\#} \mu_1, \mu_2) + d_{\text{adv}}(F_{\#} \mu_2, \mu_1) \quad (3)$$

$$+ \lambda_1 \left( \mathbb{E}_{\mu_1} [\|F(G(x)) - x\|_1] + \mathbb{E}_{\mu_2} [\|G(F(x)) - x\|_1] \right) \quad (4)$$

$$+ \lambda_2 \left( \mathbb{E}_{\mu_1} [\|F(x) - x\|_1] + \mathbb{E}_{\mu_2} [\|G(x) - x\|_1] \right), \quad (5)$$

where the distance  $d_{\text{adv}}$  (3) approximates the distance between distributions via adversarial learning (i.e., minimax learning) and approximates the pushforward constraint; the cycle consistency term (4) can be seen as a relaxation of an invertibility constraint; and the “identity” regularization (5) can be seen as a transportation cost term with  $c(x, y) = \|x - y\|_1$ . Thus, CycleGAN is approximately solving the Monge problem. StarGAN [Choi et al., 2018] generalizes CycleGAN to more than two domains. However, these approaches cannot guarantee invertibility and require expensive and challenging adversarial learning [Lucic et al., 2018, Kurach et al., 2019].

**Flow Methods** AlignFlow [Grover et al., 2020] extends CycleGAN by using invertible models so that the cycle consistency constraint is satisfied by construction:

$$\arg \min_{T_1, T_2} d_{\text{adv}}((T_2^{-1} \circ T_1)_{\#} \mu_1, \mu_2) + d_{\text{adv}}((T_1^{-1} \circ T_2)_{\#} \mu_2, \mu_1) + \lambda \left( \text{KL}(\mu_1, T_1^{-1} \alpha) + \text{KL}(\mu_2, T_2^{-1} \alpha) \right), \quad (6)$$

where the first two distance terms (equivalent to CycleGAN) are implemented using adversarial learning,  $\alpha$  is a Gaussian prior distribution, and the KL terms are implemented via maximum likelihood. The first two terms are equivalent to  $d(T_{j\#}\mu_j, T_{j'\#}\mu_{j'})$ —which aligns with the symmetric Monge pushforward constraint Eqn. 2—if the distance is invariant under invertible transformations (e.g., JSD as approximated by adversarial learning  $d_{\text{adv}}$ ). However, unlike the symmetric Monge formulation, AlignFlow ignores transportation costs entirely and pushes the shared latent representation towards the assumed prior distribution  $\alpha$  rather than the more natural barycenter distribution. Finally, for  $k > 2$ , AlignFlow would require  $\binom{k}{2}$  adversarial terms where each term adds significant complexity to training the model. Continuous normalizing flows based on solving ordinary differential equations (ODE) have added transportation costs to regularize the mappings and reduce the computational burden [Onken et al., 2020, Finlay et al., 2020]. However, these require using expensive ODE solvers whereas we focus on efficient explicitly invertible functions.

### 3 ITERATIVE ALGORITHM FOR SYMMETRIC MONGE MAP PROBLEM

To summarize the developments so far, we have cast the problem of learning a unique parsimonious shared latent representation given multiple distributions to that of solving a symmetric Monge map, which is equivalent to the OT barycenter problem. We now turn to the computational question of how to tractably estimate both the barycenter and the associated OT Monge maps from the respective class distributions to the barycenter. As mentioned in the introduction, estimating OT maps and barycenter distributions are hard in general—especially when only samples from the distributions are known—and prior deep methods require complex adversarial optimization to handle the pushforward constraint. Thus, our starting point is that for *certain classes of distributions*, the symmetric Monge map problem can be solved easily using well-known results from OT theory—thereby avoiding the need for adversarial learning. We provide specific examples of these classes of distributions and their corresponding symmetric Monge map solutions in section 4. Unfortunately, these simple classes of distributions and corresponding Monge maps may not be a good fit to the given samples, especially those in modern ML settings. Therefore, we propose an iterative approach that leverages the solutions to these simple problems at each iteration to build up a complex map one layer at a time.

At each iteration, we first estimate the respective class densities  $\{\hat{\mu}_j\}_{j=1}^k$  (possibly with shared parameters) from some carefully chosen simple classes of distributions (e.g., independent, Gaussian, density tree). We then estimate the corresponding symmetric Monge maps, denoted by  $\{t_j\}_{j=1}^k$ , which can be computed via known OT results for these simple classes of distributions. Thus, at iteration  $M$ , the transformed data correspond to transforms of the original distributions by the **deep maps**  $T_j = t_j^{(M)} \circ t_j^{(M-1)} \circ \dots \circ t_j^{(1)}$ . We summarize this meta-algorithm in Alg. 1 and provide three layer examples in section 4.

---

#### Algorithm 1 Iterative Symmetric Monge Meta-Algorithm

---

**Input:** Samples from the  $k$  class distributions  $\mathcal{X} = (X_1, X_2, \dots, X_k)$ , weight vector  $w$ , number of iterations/layers  $M$

**Output:** Estimated invertible symmetric Monge maps  $(T_1, T_2, \dots, T_k)$

```

 $T_j^{(0)} \leftarrow \text{id}, \quad \forall j$ 
for  $\ell = \{1, 2, \dots, M\}$  do
   $\hat{\mu}_1, \hat{\mu}_2, \dots, \hat{\mu}_k \leftarrow \text{EstimateClassDensities}(\mathcal{X})$ 
   $t_1, t_2, \dots, t_k \leftarrow \text{SymmetricMonge}(\hat{\mu}_1, \dots, \hat{\mu}_k)$ 
  for  $j = \{1, 2, \dots, k\}$  do
     $X_j \leftarrow t_j(X_j)$ 
     $T_j^{(\ell)} \leftarrow t_j \circ T_j^{(\ell-1)}$ 
  end for
end for
return  $(T_1^{(M)}, T_2^{(M)}, \dots, T_k^{(M)})$ 

```

---

#### 3.1 Related Iterative Approaches

Iterative Gaussianization is an iterative density estimation method, that learns invertible flow-based models [Chen and Gopinath, 2000, Lin et al., 2000, Lyu and Simoncelli, 2009, Laparra et al., 2011, Ballé et al., 2016]. The key idea is to first learn a rotation matrix via ICA [Hyvarinen, 2013] or similar method to linearly transform the data, and then Gaussianize each marginal independently. Inouye and Ravikumar [2018] extend this by iteratively building normalizing flows from more general “shallow” density estimation approaches. More recently, Sliced Iterative Generator (SIG) [Dai and Seljak, 2020] iteratively estimate an orthogonal linear transformation via sliced Wasserstein distance and then



compute optimal transport on each dimension independently. However, these prior iterative approaches are focused on density estimation (i.e., learning a generative model), and in particular, learn a mapping between a *known* base distribution (e.g. Gaussian) and the unknown data distribution. Whereas, our approach is focused on estimating a mapping between multiple *unknown* distributions to a shared latent representation.

Iterative approaches for mapping between two *unknown* distributions include Projection Pursuit Monge Map [Meng et al., 2019] that iteratively finds interesting directions to project the data onto, and estimates Monge maps for the 1D projected data. The caveat, however, is that it used fixed interestingness functions such as variance to find the projection directions. Kuang and Tabak [2019] propose an alternative iterative method for learning optimal maps and barycenters where each iteration requires the solution of a simpler but *joint* optimal transport problem—rather than solving 1D OT problems as in [Meng et al., 2019]. In practice, Kuang and Tabak [2019] use a set of fixed interestingness functions to find the needed structure. Essid et al. [2019] extend this iterative approach by using an adversarial objective to automatically learn these interestingness functions. Our approach is more general since it does not require fixed interestingness functions or adversarial training.

## 4 SYMMETRIC MONGE LAYERS

We will now develop three examples of the symmetric Monge map layers that can be used in our meta-algorithm: a) multivariate Gaussian layer, b) independent components layer, and c) decision tree layer. For each layer, we detail the two key inner-loop steps from Alg. 1: 1) estimating the class distributions given samples and 2) solving the symmetric Monge map given these class distributions.

### 4.1 Multivariate Gaussian Layer

**Multivariate Gaussian Distribution Estimators.** We merely estimate a Gaussian distribution for each class *independently*. The choice of the multivariate Gaussian estimator depends on the sampling regimes. In the small sample regime, we could choose a sparse Gaussian estimator such as graphical Lasso [Friedman et al., 2008]. If we suspect some data corruption, we could use robust Gaussian estimators such as [Cheng et al., 2019]. With enough clean samples, we can merely use the sample mean and sample covariance for each class distribution, which we use in our experiments.

**Multivariate Gaussian Symmetric Monge Maps.** Given multivariate Gaussian class distributions, we can leverage known OT results to directly solve the symmetric Monge map problem (proof in appendix).

**Theorem 2** (Optimal symmetric Monge map for Gaussian distributions). *Given  $k$  Gaussian distributions defined by their means and covariances  $\{(m_j, C_j)\}_{j=1}^k$  and a weight vector  $w$ , the optimal symmetric Monge map for Gaussian*

*distributions is:  $T_j^*(x) \equiv T_{j \rightarrow \text{bary}}^*(x) = m_{\text{bary}} + A_{j \rightarrow \text{bary}}(x - m_j)$ , where  $A_{j \rightarrow \text{bary}} \triangleq C_{\text{bary}}^{-\frac{1}{2}} (C_{\text{bary}}^{\frac{1}{2}} C_j C_{\text{bary}}^{\frac{1}{2}})^{\frac{1}{2}} C_{\text{bary}}^{-\frac{1}{2}}$ ,  $m_{\text{bary}} = \sum_{j=1}^k w_j m_j$ , and  $C_{\text{bary}}$  is the unique fixed point of the map  $\Psi(C) \triangleq \sum_{j=1}^k \sum_{j=1}^k w_j (C^{\frac{1}{2}} C_j C^{\frac{1}{2}})^{\frac{1}{2}}$ .*

### 4.2 Independent Components (Naïve) Barycenter (NB)

**Independent Component Distribution Estimators.** We propose to estimate independent class distributions with an optional shared orthogonal transformation—similar to the independent components in independent component analysis (ICA) [Hyvarinen, 2013]. More formally, we can define our independent component class distributions as:  $\forall j \in \{1, \dots, k\}$ ,  $\mu_j(x; Q, \theta_j) = \prod_{s=1}^d \mu_{js}([Qx]_s; \theta_{j,s})$ , where  $Q$  is an orthogonal matrix shared between class distributions,  $\theta_j$  are the parameters for the  $j$ -th class distribution, and  $[Qx]_s$  is the  $s$ -th coordinate after transforming  $x$  by  $Q$ . While in theory we could optimize all class distributions jointly, if  $Q$  is known, then the problem decouples into independent subproblems that can be solved very efficiently. Thus, we propose to first estimate the orthogonal transform  $Q$  (which is the more challenging part) and then estimate the independent class distributions assuming that  $Q$  is fixed.

Although we could generate a random orthogonal matrix for  $Q$ , most random directions—particularly in high-dimensional spaces—will not reveal useful structure, which will yield slow progress towards a shared representation. Thus, we seek a  $Q$  that reveals interesting structure between class distributions. We adopt the non-parametric approach of SIG that finds the orthogonal directions (or slices) that maximize the sum of 1D empirical Wasserstein distances along each direction [Dai and Seljak, 2020]. However, the formulation in Dai and Seljak [2020] only considers  $k = 2$  distributions. Thus, we generalize the approach to  $k \geq 2$  distributions by minimizing the empirical *symmetric*

Wasserstein distances inspired by our symmetric problem:

$$\arg \max_{Q: Q^T Q = I_m} \left( \sum_{j=1}^k \frac{w_k}{m} \sum_{\ell=1}^m \frac{1}{n} \sum_{i=1}^n |(X_j q_\ell)_{[i]} - Y_{[i], \ell}|^p \right)^{\frac{1}{p}}, \quad (7)$$

where  $p \geq 1$ ,  $X_j$  is the sample data matrix for the  $j$ -th class,  $(X_j q_\ell)_{[i]}$  signify the samples from the  $j$ -th class distribution projected along the direction  $q_\ell$  sorted in ascending order,  $Y_{[i], \ell} \triangleq \sum_{j=1}^k w_k (X_j q_\ell)_{[i]}$  is the empirical barycenter along direction  $q_\ell$ ,  $m \leq d$  is the number of directions, and  $I_m \in \mathbb{R}^{m \times m}$  is the identity matrix. For simplicity of exposition, we will assume that  $m = d$  for the rest of section 4 but give details for  $m < d$  in the appendix. Intuitively, this finds the directions that reveal the largest difference between class distributions along each 1D projection. Importantly, note that our optimization for  $Q$  naturally ignores any subspaces that have the same distribution among all classes—even if this shared distribution is arbitrarily complex; this yields more parsimonious transformations and preserves any shared structure in the class distributions. We adopt the approach of SIG that optimizes  $Q$  directly on the manifold of orthonormal matrices (also called a Stiefel manifold) using projected gradient descent with backtracking line search (details in Dai and Seljak [2020]).

Given the shared orthogonal matrix  $Q$ , we can now independently estimate the class distributions after projection, i.e., the class distributions of  $\mathbf{z}_j \equiv Q \mathbf{x}_j$  for all  $j \in \{1, \dots, k\}$ . Because we assume the class distributions are independent, we are free to use any univariate density estimators for each dimension independently including non-parametric estimators such as a Gaussian mixture or kernel density estimator. For high flexibility yet low computational cost, we choose to use a regularized histogram-based density estimator in our experiments (details in the appendix). We expect that any standard non-parametric estimator would work well.

**Independent Component Symmetric Monge Maps.** Given that the estimated class distributions are independent, we can leverage 1D OT results to efficiently compute the symmetric Monge map of each feature independently.

**Theorem 3** (Optimal 1D Symmetric Monge Maps). *The optimal univariate symmetric Monge maps are:  $T_j^* = F_{\text{bary}}^{-1} \circ F_j$ , where  $F_j$  is the CDF function of the  $\mu_j$  distribution and  $F_{\text{bary}}^{-1}$  is the inverse CDF of the barycenter distribution, which is known to have the following form  $F_{\text{bary}}^{-1}(u) = \sum_j w_j F_j^{-1}(u)$ .*

To account for the shared orthogonal transformation  $Q$ , we can merely pre and post process the input by  $Q$  and  $Q^T$  respectively. Thus, the joint symmetric Monge map for the  $j$ -th class can be written as:  $T_j^* = Q^T \circ [T_{j,1}^*, \dots, T_{j,d}^*]^T \circ Q$ , where  $[T_{j,1}^*, \dots, T_{j,d}^*]^T$  denotes the component-wise transformation of each coordinate and  $T_{j,s}$  is the  $j$ -th symmetric Monge map for dimension  $s$ .

### 4.3 Decision Tree Layer

To highlight that our framework can be used without gradient-based methods, we develop a decision tree layer.

**Tree Distribution Estimators.** Tree distributions are essentially multivariate generalizations of histograms with unequal bin sizes and splits based on the tree structure [Ram and Gray, 2011, Inouye and Ravikumar, 2018]. Each leaf node has a constant density value and the overall tree density is thus piecewise constant. For this layer, we will assume the data has support on the unit hypercube.<sup>1</sup>

Similar to our independent components layer, our class distributions will share the same decision tree structure, but could have different density values for the leaves, i.e., the  $j$ -th class distribution has the form:  $p_j(\mathbf{x}) = \{c_{j,\ell}, \text{ if } \mathbf{x} \in \mathcal{N}_\ell\}$ , where  $\mathcal{N}_\ell$  is the  $\ell$ -th leaf node (i.e., the shared leaf node structure) and  $c_{j,\ell}$  is the constant density value for that leaf node. Again, we choose to first estimate the shared tree structure  $\mathcal{S}_{\text{tree}} \triangleq \{\mathcal{N}_\ell\}_{\ell=1}^L$ , and then estimate the density assuming this structure is fixed. To reveal the differences between class distributions, we use a decision tree classifier to find the shared tree structure. Note that the classifier will ignore any subspaces where the class distributions are the same (even if they are arbitrarily complex) similar to the independent layer; this will encourage more parsimonious maps and a preservation of shared structure if possible. Given the shared tree structure  $\mathcal{S}_{\text{tree}}$ , the density values at each leaf node  $c_{j,\ell}$  can be estimated via the smoothed leaf node frequencies as in Inouye and Ravikumar [2018].

<sup>1</sup>If the data is not supported on the unit hypercube, the support can be modified by applying a simple preprocessor and postprocessor; for example, if the data lies in the real space, the CDF and inverse CDF of a standard normal distribution can be applied as a preprocessor and postprocessor respectively, which is what we do in our 2D experiments.

**Recursive Symmetric Monge Maps for Tree Densities.** Given the shared tree structure, we propose to estimate the symmetric Monge map by solving a sequence of 1D symmetric Monge map problems for all internal nodes in a bottom-up fashion. First, let us consider the base case of a single split. In this case, each class distribution can be viewed as a 2-bin histogram along the split dimension (while all other dimensions are assumed to be independent and uniform). Thus, we only need to solve the symmetric Monge problem for 1D histograms, which has a very efficient and closed-form solution by Theorem 3 and the theorem below for barycenters of histograms (proof in appendix). To extend to full trees, we recursively solve these 2-bin histogram problems in a bottom-up fashion where the weight vector  $w$  is proportional to the class-specific probability for the node.

**Theorem 4** (Barycenter of Histograms is a Histogram). *Given an ordered set of 1D histograms  $(\mu_{\text{hist},1}, \dots, \mu_{\text{hist},k})$  with a corresponding weight vector  $w$ , the barycenter is another a histogram with at most the number of bin edges equal to the total number of bin edges across all histograms.*

## 5 EXPERIMENTS

We explore our iterative barycenter method both qualitatively and quantitatively using both 2D simulated data and “permuted” MNIST [LeCun and Cortes, 2010]—permuted means that our methods do not leverage the image structure of MNIST but merely treat each image as 784-dimensional vector.<sup>2</sup> Additional experiments, implementation details and results can be found in the appendix, including experiments on FashionMNIST [Xiao et al., 2017].

**Metrics.** We use pushforward constraint metrics to compare fairly with prior methods, but show transportation cost to highlight that our algorithm attempts to minimize it while prior methods ignore it. We estimate the transportation cost by an average over the test set, i.e.,  $\text{TC} = \sum_{j=1}^k \frac{w_j}{n_j} \sum_{x \in X_j} \|x - \hat{T}_j(x)\|^2$ , where  $X_j$  is the test dataset for the  $j$ -th class and lower is better. While transportation cost is simple to compute, it is challenging to determine how well the pushforward constraint (i.e.,  $T_{j\#}\mu_j = T_{j'\#}\mu_{j'}, \forall j \neq j'$ ) is satisfied—a critical piece for the symmetric Monge map problem. The key issue is that we only have samples from the class distributions  $\mu_j$ . We first note that the pushforward constraint can equivalently be written as  $\mu_j = (T_j^{-1} \circ T_{j'})_{\#}\mu_{j'}, \forall j \neq j'$ . Thus, for every class distribution  $\mu_j$ , we can sample  $k-1$  “fake” distributions using our invertible transformations  $\hat{\mu}_{j' \rightarrow j} = (\hat{T}_j^{-1} \circ \hat{T}_{j'})_{\#}\mu_{j'}$ . For the 2D data, we can average the Wasserstein distance on test samples between the real and the fake distributions, i.e.,  $\text{WD} = \frac{1}{k^2 - k} \sum_{j \neq j'} \hat{W}(\mu_j, \hat{\mu}_{j' \rightarrow j})$ , where  $\hat{W}$  is the Wasserstein distance estimated using samples via the Sinkhorn algorithm with  $\epsilon = 0.1$  with maximum iterations set to 100. For higher dimensional data (e.g., MNIST), the Wasserstein distance between samples is a poor estimator of the true Wasserstein distance [Genevay et al., 2019]. Thus, we train a CNN classifier and compute the cross entropy loss between the real distribution  $\mu_j$  and a uniform mixture over fake distributions  $\bar{\mu}_{j' \rightarrow j} = \frac{1}{k-1} \sum_{j'} \hat{\mu}_{j' \rightarrow j}$  as proxy for measuring the distance between distributions, i.e.,  $\text{CEL} = \frac{1}{k} \sum_j \text{CELoss}(\mu_j, \bar{\mu}_{j' \rightarrow j}) = \frac{1}{k} \sum_j \min_f \mathbb{E}_{\mu_j} [-\log f(x)] + \mathbb{E}_{\bar{\mu}_{j' \rightarrow j}} [-\log(1 - f(x))]$ .<sup>3</sup> Higher CEL means it is harder to distinguish the real from the fake so higher is better. More details in the appendix. We compute the mean and standard deviation over 5 runs of each method. We also track approximate wall-clock training time for MNIST (all models trained on a CPU except AlignFlow which is trained on a GPU).

**Methods.** Given that there are no prior iterative approaches that map to a shared representation, we suggest a simple approach — if a normalizing flow is estimated for each class distribution *independently*, then the flows for each class can be seen to map to the same shared prior distribution. For this approach, the mappings and representations are not unique even in theory, and the shared distribution is not learned but merely assumed to be the prior distribution. However, this is the closest comparison that seems reasonable. Using this simple approach, we can compare our iterative algorithm to the flow-based iterative density estimation methods deep density destructors (DD) [Inouye and Ravikumar, 2018] and sliced iterative generator (SIG) [Dai and Seljak, 2020]. For MNIST, as a non-iterative baseline, we compare to the invertible AlignFlow [Grover et al., 2020], which explicitly maps both distributions to an assumed prior distribution. For our methods, we consider a single Gaussian barycenter (GB), a single independent (naïve) barycenter (NB), multi-layer tree barycenter (Tree), multi-layer random rotation followed by NB (Rand-NB), multi-layer orthogonal transform found using max sliced Wasserstein distance (subsection 4.2) followed by NB (mSWD-NB). Number of layers and other parameters are in the appendix.

**2D experiments.** The qualitative results in Fig. 1 illustrate that our methods (Tree, mSWD-NB) find shared latent spaces closer to the barycenter distribution (since the transportation cost is low) whereas density destructors (DD)

<sup>2</sup>AlignFlow and the CNN classifier we use for evaluation do use the image structure but our iterative methods do not.

<sup>3</sup>While in theory we could compute the cross entropy loss for every pair of class distributions, we do not consider that here because of the computational cost—each cross entropy loss term requires training a CNN classifier.

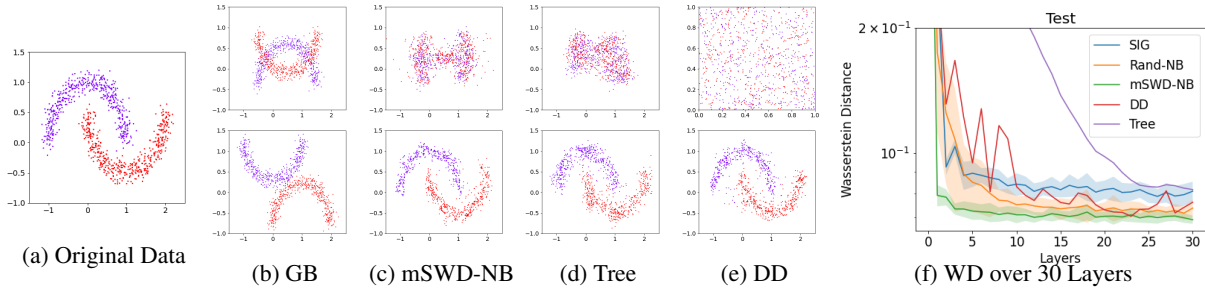


Figure 1: The shared representations (top row) for each method show that our iterative methods (DD, Tree) find low transportation cost shared latent spaces whereas DD ignores transportation cost and merely projects both distributions to the uniform distribution. The bottom row shows test samples that were flipped to the other class distribution (ideally these “fake” samples would look like the original data).

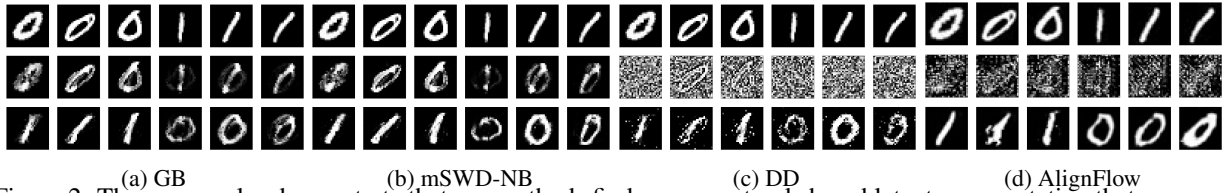


Figure 2: These examples demonstrate that our methods find a more natural shared latent representation that preserves structural similarities (e.g., black pixels) between the two digits while DD and AlignFlow do not. The rows from top to bottom are the original MNIST digits, their latent representation, and their projection to the space of the other digit (i.e., flipped).

ignores transportation costs and projects both distributions to the uniform distribution. The results for the 2D datasets with  $k = 2$  in Table 1 demonstrate that our iterative barycenter flows perform comparable or better than the baseline methods (DD, SIG) in terms of the pushforward constraint, which is measured by the empirical Wasserstein-2 distance on test data (WD), while having significantly lower transportation cost (TC) on test data. Additional experiments and results for  $k > 2$  in appendix.

Table 1: Transportation cost (TC), sample-based Wasserstein distance (WD, lower is better) for 2D data. More 2D datasets in appendix.

Dataset	Moon			
Model	TC	Std	WD	Std
GB	<b>0.400</b>	<b>0.000</b>	0.271	0.000
NB	0.401	0.000	0.268	0.000
Rand-NB	0.480	0.014	0.075	0.007
mSWD-NB	0.463	0.012	<b>0.069</b>	<b>0.002</b>
Tree	0.540	0.003	0.079	0.001
DD	1.256	0.000	0.075	0.000
SIG	1.675	0.090	0.079	0.010

**“Permuted” MNIST.** Qualitative samples from the latent space and after flipping between the two digits (Fig. 2) highlight that our barycenter methods retain shared latent structure such as the black pixels, whereas the generative baselines (DD, AlignFlow) try to move the shared latent distribution to the assumed prior (uniform or Gaussian, respectively) so that shared structure is also removed. To emphasize that our method can scale to more class distributions, we present qualitative examples of transforming between every digit and every other digit (i.e.,  $k = 10$ ) for MNIST in Fig. 3 (quantitative results in appendix). In Fig. 3, real samples are along the diagonal and each column shows the mapping to another digit distribution (e.g., the bottom left “9” image is the mapping of the real sample “0” on the top left). Notice that even for this multiclass case, almost all transformed digits are recognizable. This multi-class situation (i.e.  $k > 2$ ) is much more difficult for AlignFlow (which did not implement  $k > 2$ ) and would naïvely require  $k^2 - k$  pairwise adversarial loss terms. We emphasize that our extension to  $k > 2$  is straightforward because we only need to solve simple symmetric Monge map problems, which scale linearly with  $k$ . The results for  $k = 2$  in Table 2 show that our methods perform well in terms of the pushforward constraint (measured by the CNN cross-entropy loss where higher is better) while having significantly lower transportation costs (TC) than the iterative baseline (DD) and

Table 2: Transportation cost (TC), cross entropy loss (CEL, higher is better) and time for MNIST.

Dataset Model	MNIST(k=2)				
	TC	Std	CEL	Std	Time(s)
GB	<b>25.0</b>	<b>0.000</b>	0.316	0.021	50
NB	28.1	0.000	0.004	0.001	<b>25</b>
Tree	29.9	0.247	0.005	0.002	3800
mSWD-Tree	44.6	0.269	0.004	0.001	1800
mSWD-NB	32.9	0.048	<b>0.682</b>	<b>0.003</b>	2200
DD	235.2	0.000	0.028	0.007	360
AlignFlow ( $\lambda=1e-4$ )	303.6	-	0.121	-	39200
AlignFlow ( $\lambda=1e-5$ )	353.2	-	0.021	-	39200

end-to-end baseline AlignFlow. Also, the computational cost is much lower for the iterative methods ( $< 1.5$  hour on CPU), whereas AlignFlow trained for 50 epochs on a GPU took approximately 11 hours (thus, we only estimate one model and cannot compute standard deviations for AlignFlow). While the tree approach performed comparably in low dimensions, the tree approach performs poorly in this high-dimensional setting.

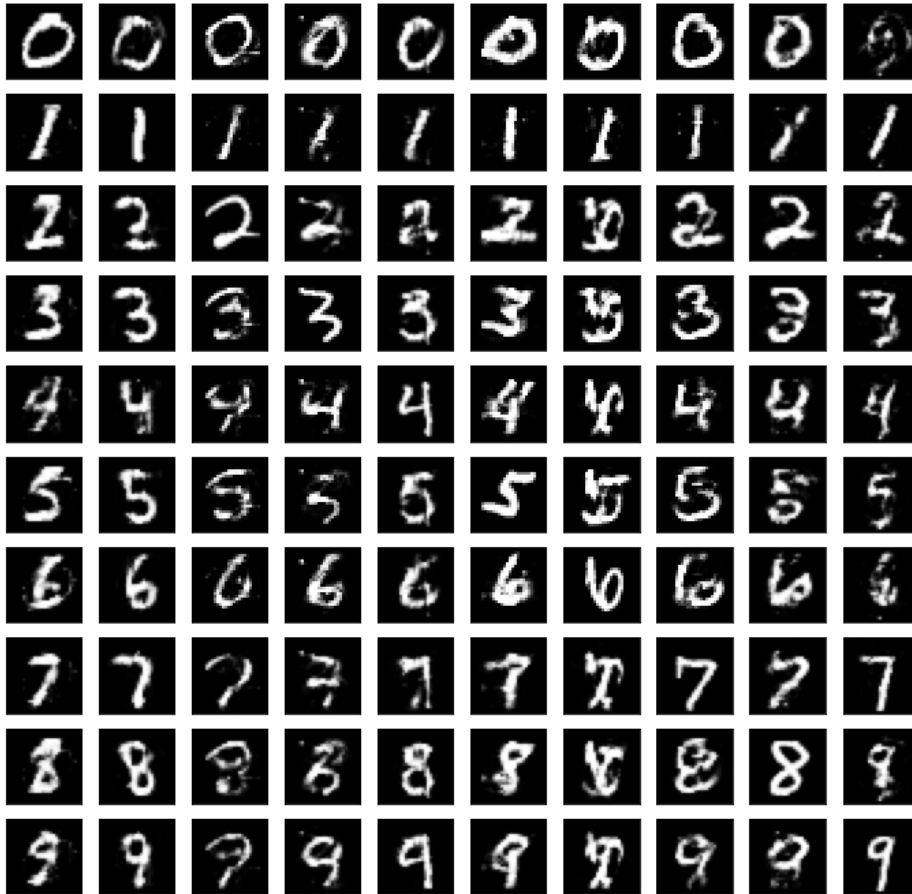


Figure 3: Multi-domain ( $k = 10$ ) results for MNIST with mSWD-NB. The diagonal shows the real samples and each column shows the mappings of the real sample to the distribution of the other digits.

## 6 DISCUSSION AND CONCLUSION

We seek to estimate the maps between two or more distributions and a unique and parsimonious shared latent representation. We formulate the symmetric Monge map problem and prove that it maps to the natural barycenter distribution—a result that may be of independent interest. Unlike normalizing flows or standard generative approaches, our formulation does not require a pre-fixed latent distribution but can be applied to any two *unknown* distributions. However, this requires solving a very challenging OT problem both theoretically and computationally. Therefore, we leverage OT theory and insights from modern density estimation to construct a practical iterative estimation algorithm.

Specifically, each iteration of our algorithm adds a layer to our model by first estimating the class distributions and then estimating the symmetric Monge map for this problem using known OT results. Unlike prior methods, our approach enables efficient *multi-class* distribution mappings to a shared representation (e.g., see Fig. 3). More generally, our iterative approach can also provide a complementary perspective for solving challenging deep learning problems because it is computationally efficient and does not require end-to-end learning, gradient-based methods, or adversarial optimization. In our experiments, we see that the shared latent space indeed seems qualitatively better than alternatives because it preserves some shared structure (Fig. 2).

We believe our work is a first step that can open up novel perspectives, algorithms, and theory. For example, we expect that the sample complexity of our symmetric Monge problem will be lower than normalizing flow approaches such as AlignFlow or density destructors. To build intuition, consider that images lie on lower dimensional curves. Normalizing flows would need to transform these curves to a Gaussian or uniform distribution over the entire ambient image space. However, the symmetric Monge problem would only have to transform both distributions to some shared barycenter curves. If the images share structure, these curves will be much closer to each other than a Gaussian distribution. We leave development of this theory to future work.

Despite many advantages of our approach, however, there are also many open challenges. For example, can we guarantee that each iteration of our algorithm reduces some statistical distance between the distributions similar to what has been proved for iterative Gaussianization? While we initially attempted to prove this, we believe theoretical guarantees of our iterative algorithm to be much more challenging than iterative Gaussianization because the class distributions are assumed to be *unknown* except through samples (while Gaussianization assumes one distribution is a known prior distribution). Given the generality of the class distributions, we expect that while counterexamples likely exist (thereby excluding simple proofs), these worst cases are uncommon in practice given our experimental results. We expect that modern smoothed analysis could enable proofs of convergence beyond simple worst-case analysis, but this will require significant theoretical development so we leave this to future work. Another theoretical challenge is proving approximation bounds on how well the iterative algorithm approximates the true barycenter. While our experiments demonstrate that the approximation error is reasonable in practice, providing bounds for our iterative algorithm even under certain regularity conditions of the unknown class distributions would be an excellent future direction. Thus, we believe that our formulation as a symmetric Monge problem and our iterative algorithm open up new theoretical and fundamental questions.

## Acknowledgments

D.I., Z.Z., and Z.G. acknowledge support from the Army Research Lab through contract number W911NF-2020-221. P. R. acknowledges the support of NSF via IIS-1909816.

## References

- Martial Agueh and Guillaume Carlier. Barycenters in the wasserstein space. *SIAM Journal on Mathematical Analysis*, 43(2):904–924, 2011.
- Johannes Ballé, Valero Laparra, and Eero P. Simoncelli. Density modeling of images using a generalized normalization transformation. *ICLR*, pages 1–12, 2016.
- Scott Shaobing Saobing Chen and Ramesh A. Gopinath. Gaussianization. *NIPS*, pages 423–429, 2000.
- Yu Cheng, Ilias Diakonikolas, Rong Ge, and David Woodruff. Faster algorithms for high-dimensional robust covariance estimation, 2019.
- Yunjey Choi, Minje Choi, Munyoung Kim, Jung-Woo Ha, Sunghun Kim, and Jaegul Choo. Stargan: Unified generative adversarial networks for multi-domain image-to-image translation. In *Proceedings of the IEEE conference on computer vision and pattern recognition*, pages 8789–8797, 2018.
- Biwei Dai and Uros Seljak. Sliced iterative generator, 2020.
- Laurent Dinh, Jascha Sohl-Dickstein, and Samy Bengio. Density estimation using real nvp. In *International Conference on Learning Representations*, 2017.
- Montacer Essid, Debra F Laefer, and Esteban G Tabak. Adaptive optimal transport. *Information and Inference: A Journal of the IMA*, 8(4):789–816, 2019.
- Chris Finlay, Jorn Jacobsen, Levon Nurbekyan, and Adam Oberman. How to train your neural ode: The world of jacobian and kinetic regularization. In *International Conference on Machine Learning (ICML)*, 2020.
- J. Friedman, T. Hastie, and R. Tibshirani. Sparse inverse covariance estimation with the graphical lasso. *Biostatistics*, 9(3):432–441, jul 2008.
- Aude Genevay, Lénaïc Chizat, Francis Bach, Marco Cuturi, and Gabriel Peyré. Sample complexity of sinkhorn divergences, 2019.
- Aditya Grover, Christopher Chute, Rui Shu, Zhangjie Cao, and Stefano Ermon. Alignflow: Cycle consistent learning from multiple domains via normalizing flows. In *AAAI*, 2020.
- Laleh Haghverdi, Aaron TL Lun, Michael D Morgan, and John C Marioni. Batch effects in single-cell rna-sequencing data are corrected by matching mutual nearest neighbors. *Nature biotechnology*, 36(5):421–427, 2018.
- Lanqing Hu, Meina Kan, Shiguang Shan, and Xilin Chen. Duplex generative adversarial network for unsupervised domain adaptation. In *Proceedings of the IEEE Conference on Computer Vision and Pattern Recognition (CVPR)*, June 2018.
- Aapo Hyvarinen. Independent component analysis: recent advances. *Philosophical Transactions of the Royal Society A: Mathematical, Physical and Engineering Sciences*, 371(1984), 2013. doi: 10.1098/rsta.2011.0534. URL <https://royalsocietypublishing.org/doi/abs/10.1098/rsta.2011.0534>.
- David I. Inouye and Pradeep Ravikumar. Deep density destructors. In *International Conference on Machine Learning (ICML)*, pages 2172–2180, jul 2018.
- Durk P Kingma and Prafulla Dhariwal. Glow: Generative flow with invertible 1x1 convolutions. In *Advances in neural information processing systems*, pages 10215–10224, 2018.
- Durk P Kingma, Tim Salimans, Rafal Jozefowicz, Xi Chen, Ilya Sutskever, and Max Welling. Improved variational inference with inverse autoregressive flow. In *Advances in neural information processing systems*, pages 4743–4751, 2016.
- Max Kuang and Esteban G Tabak. Sample-based optimal transport and barycenter problems. *Communications on Pure and Applied Mathematics*, 72(8):1581–1630, 2019.
- Karol Kurach, Mario Lucic, Xiaohua Zhai, Marcin Michalski, and Sylvain Gelly. The GAN landscape: Losses, architectures, regularization, and normalization, 2019. URL <https://openreview.net/forum?id=rkGG6s0qKQ>.
- Valero Laparra, Gustavo Camps-Valls, and Jesús Malo. Iterative Gaussianization: From ICA to random rotations. *IEEE Transactions on Neural Networks*, 22(4):537–549, 2011.
- Yann LeCun and Corinna Cortes. MNIST handwritten digit database. <http://yann.lecun.com/exdb/mnist/>, 2010. URL <http://yann.lecun.com/exdb/mnist/>.
- J.J. Lin, N. Saito, and R.A. Levine. An iterative nonlinear Gaussianization algorithm for resampling dependent components. *Proc. 2nd International Workshop on Independent Component Analysis and Blind Signal Separation*, pages 245–250, 2000.

- Mario Lucic, Karol Kurach, Marcin Michalski, Sylvain Gelly, and Olivier Bousquet. Are gans created equal? a large-scale study. In *Advances in neural information processing systems*, pages 700–709, 2018.
- Siwei Lyu and Eero P Simoncelli. Nonlinear extraction of independent components of natural images using radial Gaussianization. *Neural computation*, 21:1485–1519, 2009.
- Cheng Meng, Yuan Ke, Jingyi Zhang, Mengrui Zhang, Wenxuan Zhong, and Ping Ma. Large-scale optimal transport map estimation using projection pursuit. In H. Wallach, H. Larochelle, A. Beygelzimer, F. d’Alché-Buc, E. Fox, and R. Garnett, editors, *Advances in Neural Information Processing Systems 32*, pages 8118–8129. Curran Associates, Inc., 2019.
- Derek Onken, Samy Wu Fung, Xingjian Li, and Lars Ruthotto. Ot-flow: Fast and accurate continuous normalizing flows via optimal transport. *arXiv preprint arXiv:2006.00104*, 2020.
- Gabriel Peyré and Marco Cuturi. Computational optimal transport. *Foundations and Trends<sup>®</sup> in Machine Learning*, 11(5-6):355–607, 2019. ISSN 1935-8237. doi: 10.1561/22000000073. URL <http://dx.doi.org/10.1561/22000000073>.
- Parikshit Ram and Alexander G Gray. Density estimation trees. In *KDD*, pages 627–635, 2011.
- Vivien Seguy, Bharath Bhushan Damodaran, Remi Flamary, Nicolas Courty, Antoine Rolet, and Mathieu Blondel. Large scale optimal transport and mapping estimation. In *International Conference on Learning Representations*, 2018.
- Han Xiao, Kashif Rasul, and Roland Vollgraf. Fashion-mnist: a novel image dataset for benchmarking machine learning algorithms, 2017.
- Rich Zemel, Yu Wu, Kevin Swersky, Toni Pitassi, and Cynthia Dwork. Learning fair representations. In Sanjoy Dasgupta and David McAllester, editors, *International Conference on Machine Learning*, volume 28 of *Proceedings of Machine Learning Research*, pages 325–333, Atlanta, Georgia, USA, 17–19 Jun 2013.
- Jun-Yan Zhu, Taesung Park, Phillip Isola, and Alexei A Efros. Unpaired image-to-image translation using cycle-consistent adversarial networks. In *Computer Vision (ICCV), 2017 IEEE International Conference on*, 2017.



## A OVERVIEW

We have organized our appendix as follows:

- Appendix B includes the proofs (and key OT results needed for the proofs).
- Appendix C describes additional experiments including additional FashionMNIST experiments and includes quantitative result tables for these experiments (qualitative figures are included in the final appendix section).
- Appendix D provides more details on our experimental setup including dataset preparation, models, and metric details.
- Appendix E provides both expanded figures from the main paper and new result figures for the additional experiments.

## B PROOFS

*Proof of Theorem 1.* First, let us denote  $\nu \triangleq T_{j*}^* \mu_j$  for any  $j$  since they are all equal because of the pushforward condition (at this point we do not assume anything about  $\nu$ ). We can prove that  $T_j^*$  is the optimal Monge map (which is unique for quadratic cost) from  $\mu_j$  to  $\nu$  for all  $j$ , i.e.,  $T_j^* = T_{j \rightarrow \nu}^*$ , via contradiction. Suppose  $T^* \neq T_{j \rightarrow \nu}^*$ , then  $T^*$  could be replaced by the optimal Monge map and the minimum value could be reduced—which is a contradiction to the optimality of  $T^*$ . Given this fact and Brenier’s theorem [Peyré and Cuturi, 2019, Theorem 2.1] on the equivalence between the Kantorovich and the Monge map problems, we can now transform our original objective at the optimum  $T_j^*$  to the Kantorovich barycenter objective from Def. 4 at its optimum:

$$\sum_{j=1}^k w_j \int_{\mathcal{X}_j} c(x, T_j^*(x)) d\mu_j(x) \quad (8)$$

$$= \sum_{j=1}^k w_j \int_{\mathcal{X}_j \times \mathcal{Y}} c(x, y) d\pi_j^*(x, y) \quad (9)$$

$$= \sum_{j=1}^k w_j \min_{\pi_j \in \mathcal{U}(\mu_j, \nu)} \int_{\mathcal{X}_j \times \mathcal{Y}} c(x, y) d\pi_j(x, y) \quad (10)$$

$$= \sum_{j=1}^k w_j \mathcal{L}_c(\nu, \mu_j), \quad (11)$$

where the first equality is by Brenier’s theorem, the second equality is by the definition of the Kantorovich problem, and the third equality is by the definition of  $\mathcal{L}_c$ . Thus, our objective can be equivalently written as optimizing over  $\nu$  for the objective above, which is exactly the definition of a barycenter in Def. 4. Thus,  $\nu = \text{bary}(\mu_1, \mu_2, \dots, \mu_k; \mathbf{w})$ .  $\square$

**Proposition 5** (Optimal transport map between Gaussian distributions [Peyré and Cuturi, 2019, Remark 2.31]). *The optimal transport map between two Gaussian distributions defined by parameters  $\{(\mu_1, \Sigma_1), (\mu_2, \Sigma_2)\}$  is a simple linear map:*

$$T_{1 \rightarrow 2}^*(\mathbf{x}) = \mu_2 + A(\mathbf{x} - \mu_1), \quad (12)$$

where  $A \triangleq \Sigma_1^{-\frac{1}{2}} (\Sigma_1^{\frac{1}{2}} \Sigma_2 \Sigma_1^{\frac{1}{2}})^{\frac{1}{2}} \Sigma_1^{-\frac{1}{2}} = A^T$ .

**Proposition 6** (Barycenter of Gaussian distributions [Peyré and Cuturi, 2019, Remark 9.5]). *Given  $k$  Gaussian distributions defined by parameters  $\{(\mu_j, \Sigma_j)\}_{j=1}^k$  and a weight vector  $\mathbf{w}$ , the barycenter of Gaussian distributions is a Gaussian distribution with where the mean is  $\mu = \sum_{j=1}^k w_j \mu_j$  and the covariance is the unique positive definite fixed point of the map:*

$$\Sigma^* = \Psi(\Sigma^*) \text{ where } \Psi(\Sigma) \triangleq \sum_{j=1}^k \sum_{j=1}^k w_j (\Sigma^{\frac{1}{2}} \Sigma_j \Sigma^{\frac{1}{2}})^{\frac{1}{2}}, \quad (13)$$

where  $\Sigma^{\frac{1}{2}}$  is the square root of positive semidefinite matrices.

*Proof of Theorem 2.* From Theorem 1, we know that the solution the symmetric Monge problem is the Monge map between the class distribution and the barycenter distribution. From Proposition 6, we can form the Gaussian barycenter

distribution given the class distributions. We can then combine this result with Proposition 5 to solve for the optimal map between the Gaussian class distribution and the Gaussian barycenter distribution. By inspection, this optimal map is the one stated in Theorem 2.  $\square$

**Proposition 7** (Univariate Barycenter [Peyré and Cuturi, 2019, Remark 9.6]). *Given a weight vector  $w$  with cost  $c(x, y) = \|x - y\|^2$ , the inverse CDF of the barycenter is the weighted average inverse CDF of the class distributions, i.e.,*

$$\forall u \in [0, 1], \quad F_{\text{bary}}^{-1}(u) = \sum_{j=1}^k w_j F_j^{-1}(u), \quad (14)$$

where  $F_j^{-1}$  is the inverse CDF of the  $j$ -th class distribution.

**Proposition 8** (Univariate Optimal Transport Map [Peyré and Cuturi, 2019, Remark 2.30]). *The optimal map between univariate distributions  $\alpha$  and  $\beta$  is the composition of the CDF of  $\alpha$  with the inverse CDF of  $\beta$ , i.e.,*

$$T_{\alpha \rightarrow \beta}^* = F_{\beta}^{-1} \circ F_{\alpha}. \quad (15)$$

*Proof of Theorem 3.* Similar to the proof for Theorem 2, we can simply combine the equivalence of symmetric Monge maps to the barycenter problem in Theorem 1 with the known 1D results above in Proposition 7 and Proposition 8 to arrive at the corollary.  $\square$

*Proof of Theorem 4.* Because histograms are piecewise constant densities, we know that their corresponding CDFs are piecewise linear. Thus, the inverse CDFs are also piecewise linear. The barycenter inverse CDF is a simple linear combination of component inverse CDFs via Proposition 7. And, the linear combination of piecewise linear functions is also a piecewise linear function. Thus, the barycenter inverse CDF is a piecewise linear function. Because the barycenter inverse CDF is a piecewise linear function, the barycenter corresponds to a histogram. Additionally, the number of changes in the piecewise linear function can only be less than or equal to the number of changes (i.e., bin edges) in all the class histograms combined.  $\square$

## C ADDITIONAL EXPERIMENTS

In this section, we include the quantitative results for all experiments in addition to those presented in the main paper. In the following subsections, brief introductions of each experiment are provided. More experiment details are provided in the next section.

### C.1 2D Experiment for All Datasets

For the 2D datasets with  $k = 2$ , we investigate the performance of our iterative methods along with the baselines DD and SIG. For  $k > 2$ , we only compare to DD because it performs better or comparable to SIG in most of our experiments. See Table 3 and Table 4 for quantitative results. See Figure 4, Figure 15, Figure 16 and Figure 17 for expanded figures of the latent representation and translations between distributions. In both  $k = 2$  and  $k > 2$  cases, our iterative models especially mSWD-NB successfully translate the distributions to look similar to the original data (i.e., the fake distributions by translating from one class to another are similar to the original distributions). GB only works well for Gaussian distribution which it is designed to work with while NB works badly with all distributions. DD also finds the flipped distribution but it finds a less natural shared representation. Tree works well for simple task such as concentric circles with  $k = 2$  but in general it does not perform as well so we do not compare to Tree in future experiments.

### C.2 FashionMNIST with $k = 2$ Class Distributions

We redo the experiment for MNIST with  $k = 2$  in the main paper for FashionMNIST with  $k = 2$ . See Table 5 for quantitative result. See Figure 7 and Figure 8 for expanded figures of MNIST and FashionMNIST. For fairness, we simply pick the first three samples in test set here. These examples demonstrate that our methods find a more natural shared latent representation that preserves structural similarities (e.g., black pixels) between the two digits while DD and AlignFlow do not preserve this shared structure.

### C.3 MNIST and FashionMNIST with $k = 3$ Class Distributions

We investigate the performance of our models together with DD for more than two class distributions. See Table 6 for quantitative result. See Figure 5 and Figure 6 for mapping performance. For fairness, we pick the first sample in test set here. See Figure 9 and Figure 10 for more samples of latent representation of each method. The latent representation of our models keeps more features of original samples while DD just projects to uniform distribution.

### C.4 MNIST with $k = 10$ Class Distributions

We investigate the performance of our models together with DD for ten class distributions. See Table 7 for quantitative result. See Figure 11 for latent representation of each digit. See Figure 12, Figure 13 and Figure 14 for expanded figures of mapping performance with different models. For fairness, we pick the first sample in test set here. We can observe that with mSWD-NB, most mappings seem good though the model struggles to translate in certain cases such as from 6 to 8.

Table 3: Transportation cost (TC), sample-based Wasserstein distance (WD, lower is better) for 2D data. The best methods (within one standard deviation of the top method) are bolded.

Dataset Model	Moon				Random Pattern				Circles			
	TC	Std	WD	Std	TC	Std	WD	Std	TC	Std	WD	Std
GB	<b>0.400</b>	<b>0.000</b>	0.271	0.000	<b>0.923</b>	<b>0.000</b>	0.323	0.000	<b>0.059</b>	<b>0.000</b>	0.077	0.000
NB	0.401	0.000	0.268	0.000	0.954	0.000	0.460	0.000	0.060	0.000	0.075	0.000
Rand-NB	0.480	0.014	0.075	0.007	1.067	0.040	<b>0.209</b>	<b>0.064</b>	0.086	0.006	0.079	0.003
mSWD-NB	0.463	0.012	<b>0.069</b>	<b>0.002</b>	1.020	0.032	<b>0.204</b>	<b>0.060</b>	0.088	0.005	0.076	0.003
Tree	0.540	0.003	0.079	0.001	0.989	0.000	0.260	0.000	0.069	0.000	<b>0.072</b>	<b>0.000</b>
DD	1.256	0.000	0.075	0.000	3.700	0.000	<b>0.188</b>	<b>0.000</b>	1.258	0.000	0.081	0.000
SIG	1.675	0.090	0.079	0.010	1.688	0.120	0.410	0.123	0.600	0.028	0.077	0.001

Table 4: The results for the 2D random pattern dataset with  $k = 4$  and 2D Gaussian with  $k = 3$  demonstrate that our methods still perform well for  $k > 2$  in terms of the pushforward constraint, which is measured by the empirical Wasserstein-2 distance on test data (WD), while having significantly lower transportation cost (TC) for test data. The best methods (within one standard deviation of the top method) are bolded.

Dataset Model	Random Pattern (k=4)				Gaussian (k=3)			
	TC	Std	WD	Std	TC	Std	WD	Std
GB	8.928	0.000	1.315	0.000	7.455	0.000	0.533	0.000
NB	9.084	0.000	1.157	0.000	7.027	0.000	3.015	0.000
Rand-NB	9.564	0.061	<b>0.418</b>	<b>0.035</b>	7.479	0.016	<b>0.511</b>	<b>0.006</b>
mSWD-NB	9.545	0.023	<b>0.447</b>	<b>0.049</b>	7.461	0.006	<b>0.513</b>	<b>0.004</b>
Tree	<b>7.736</b>	<b>0.000</b>	1.613	0.000	<b>5.979</b>	<b>0.000</b>	0.600	0.000
DD	9.434	0.000	0.636	0.000	7.851	0.000	0.562	0.000

Table 5: Expanded results for MNIST and FashionMNIST with  $k = 2$ . The best methods (within one standard deviation of the top method) are bolded.

Dataset Model	MNIST(k=2)					FMNIST(k=2)				
	TC	Std	CEL	Std	Time(s)	TC	Std	CEL	Std	Time(s)
GB	<b>24.975</b>	<b>0.000</b>	0.316	0.021	50	21.602	0.000	0.097	0.008	40
NB	28.115	0.000	0.004	0.001	<b>25</b>	<b>20.522</b>	<b>0.000</b>	0.025	0.004	<b>20</b>
Tree	29.888	0.247	0.005	0.002	3800	21.717	0.174	0.014	0.004	4300
mSWD-Tree	44.597	0.269	0.004	0.001	1800	87.597	6.417	0.011	0.005	2300
mSWD-NB	32.906	0.048	<b>0.682</b>	<b>0.003</b>	2200	26.971	0.097	<b>0.108</b>	<b>0.008</b>	1900
DD	235.164	0.000	0.028	0.007	360	181.401	0.000	0.039	0.013	320
AlignFlow ( $\lambda=1e-4$ )	303.633	-	0.121	-	39200	445.098	-	<b>0.104</b>	-	39200
AlignFlow ( $\lambda=1e-5$ )	353.219	-	0.021	-	39200	242.400	-	0.056	-	39200

Table 6: Results for MNIST and FashionMNIST with  $k = 3$ . It shows that our method enables a natural extension beyond the two class case without requiring a significant increase in computational complexity. The best methods (within one standard deviation of the top method) are bolded.

Dataset Model	MNIST(k=3)					FMNIST(k=3)				
	TC	Std	CEL	Std	Time(s)	TC	Std	CEL	Std	Time(s)
GB	<b>22.954</b>	<b>0.002</b>	0.201	0.017	260	<b>26.375</b>	<b>0.004</b>	0.073	0.007	280
NB	28.958	0.000	0.005	0.001	<b>30</b>	28.233	0.000	0.011	0.002	<b>30</b>
GBNB	32.385	0.003	0.115	0.009	290	31.711	0.006	0.070	0.008	330
mSWD-NB	34.046	0.068	<b>0.657</b>	<b>0.008</b>	4300	35.864	0.075	<b>0.129</b>	<b>0.017</b>	4600
DD	233.354	0.000	0.035	0.008	430	171.149	0.000	0.056	0.002	490

Table 7: Our results for MNIST with  $k = 10$  digits show that our method enables a natural extension beyond the two class case without requiring a significant increase in computational complexity. The best methods (within one standard deviation of the top method) are bolded.

Dataset Model	MNIST(k=10)				
	TC	Std	CEL	Std	Time(s)
GB	<b>16.234</b>	<b>0.001</b>	0.188	0.010	1000
NB	25.907	0.000	0.024	0.002	<b>120</b>
GBNB	28.143	0.001	0.131	0.006	1150
mSWD-NB	28.989	0.093	<b>0.534</b>	<b>0.007</b>	3400
DD	227.171	0.000	0.041	0.003	1800

## D EXPERIMENT DETAILS

### D.1 Histogram-based 1D Density Estimators for NB Method

For high flexibility yet low computational cost, we choose to use a histogram-based density estimator for our independent component (naïve) layers (NB) in our experiments. While histograms are generally efficient and reasonable non-parametric estimators, one key drawback is that you must choose the interval for the histogram (e.g., using the minimum and maximum of the data). This can yield odd edge conditions if the interval is not chosen properly. Thus, to avoid this challenge, we first estimate a preprocessing transformation to squeeze the data to the interval  $[0, 1]$  and then estimate a histogram on this fixed interval. In particular, we merely use a Gaussian CDF (where the mean and covariance are estimated from the data) to preprocess the data. We then estimate a histogram on the transformed data. This can be seen as an almost trivial 1D normalizing flow where the histogram is a learned base prior distribution and the Gaussian CDF is the flow. We use the code from deep density destructors [Inouye and Ravikumar, 2018] to implement this estimation procedure. Note that this estimation procedure only requires estimating a 1D Gaussian and a 1D histogram—both of which have minimal computational cost.

### D.2 Details when the number of target directions is less than the dimensionality ( $m < d$ )

For the independent components layer, if the number of target directions  $m$  is less than the dimensionality  $d$ , we can define a partial independent components layer that only acts on  $m$  directions. From a theoretical viewpoint, we could adjust our estimators as follows:

1. For estimating  $Q$ , the other  $d - m$  directions of  $Q$  can be filled in with an arbitrary orthonormal subspace.
2. When estimating the independent class distributions, we could assume that the  $d - m$  directions have the same distribution for *all* classes.

The first assumption allows us to preserve the full dimensionality of the data when projecting into the latent space. The second assumption implies that the transform along the  $d - m$  directions is the identity because all the class distributions are the same, which implies that their barycenter is equal to the class distributions, which implies that the symmetric Monge map is merely the identity function (see Proposition 8). Thus, it can be seen that these assumptions roughly just ignore the  $d - m$  directions.

In practice, we do not have to actually create a full orthogonal matrix  $Q$  or estimate the class distributions along the other  $d - m$  directions. We can instead use truncated orthogonal matrices (i.e., where the columns are orthogonal but it is not square) and truncated joint transformations. More formally, we can create the following invertible but “truncated” transform to avoid unnecessary computation as is done in [Dai and Seljak, 2020]:

$$T_j^*(\mathbf{x}) = Q \circ [T_{j,1}^*, \dots, T_{j,m}^*] \circ Q(\mathbf{x}) + \mathbf{x}^\perp = Q \circ [T_{j,1}^*, \dots, T_{j,m}^*] \circ Q(\mathbf{x}) + (\mathbf{x} - QQ^T\mathbf{x}), \quad (16)$$

where  $\mathbf{x}^\perp \triangleq \mathbf{x} - QQ^T\mathbf{x}$  contains the components that are perpendicular to  $Q$ . Note that this transformation is invertible and equivalent to the non-truncated “theoretical” version described above but requires significantly less computation.

### D.3 Datasets

In each run of our experiments, we use the same data even for our simulated data (i.e., we use the same random seed for generating the data for each run).

**2D distributions** For 2D data, we use the fixed samples for each repetition of experiment (i.e., we produce simulated data for all runs rather than producing new simulated data for each run).

- $k = 2$ : Datasets of Moon, Random Pattern, Circles are generated by `make_moons`, `make_classification` and `make_circles` in `sklearn.datasets` respectively. The original number of training samples is 2000 and the original number of test samples is 1000.
- $k > 2$ : Dataset of Random Pattern ( $k = 4$ ) is generated by `make_classification` in `sklearn.datasets`. The original number of training samples is 2666 and the original number of test samples is 1334. Dataset of Gaussian ( $k = 3$ ) is generated by `MultivariateNormal` in `torch.distributions.multivariate_normal` with different means and covariances. The original number of training samples is 4000 and the original number of test samples is 2000.

**MNIST and FashionMNIST** We first take the full MNIST dataset (70k samples) and split into training and testing split. The dimensionality of MNIST and FashionMNIST datasets is 784. To ensure all classes have the same number of

samples in the training and test split, we take the minimum number of samples over all classes and truncate the samples of all digits to that number. The numbers vary slightly depending on the number of class distributions  $k$  and datasets but are approximately 4500 samples per digit for training and 2300 samples per digit for testing (Experiment for MNIST with  $k = 10$  has approximately 1800 samples per digit for testing). For the evaluation of the cross entropy loss, we use the first 1500 samples per digit in the test set to train the CNN classifier and the remaining samples to evaluate the cross entropy loss. For each run of the experiment, we use the same truncated datasets.

For our models including DD, we preprocess the data by dequantizing the original data with uniform distribution and dividing by 256 to create a continuous distribution over the unit hypercube. For AlignFlow, the data is further normalized to the range  $[-1, 1]$  to serve as the input to the Real-NVP and the GAN discriminator as in the original AlignFlow paper.

See below for the exact classes we use for our experiments.

- MNIST with  $k = 2$ : We use digit 0 and 1.
- FashionMNIST with  $k = 2$ : We use T-shirt and trouser.
- MNIST with  $k = 3$ : We use digit 0, 1 and 9.
- FashionMNIST with  $k = 3$ : We use T-shirt, trouser and pullover.
- MNIST with  $k = 10$ : We use digit 0-9.

#### D.4 Models for 2D Experiments

##### Two class distributions ( $k = 2$ )

- Number of layers: All iterative models (including mSWD-NB, NB-mSWD-NB, Rand-NB, NB-Rand-NB, DD, SIG) use 15 layers with the exception of the Tree method in which we used 50 highly-regularized layers (similar to [Inouye and Ravikumar, 2018] where the tree layers are highly regularized).
- Number of dimensions for orthogonal transformation: We apply orthogonal transformation in the full space with dimension 2, i.e.,  $m = d = 2$ .
- mSWD-NB: We iteratively fit NB after orthogonal transformation based on max sliced Wasserstein distance.
- Rand-NB: We iteratively fit NB after random orthogonal transformation found by QR decomposition of a matrix generated by `torch.randn`.
- NB-mSWD-NB and NB-Rand-NB: We first perform a full-dimensional NB layer and then follow this by 14 iterations of mSWD-NB/Rand-NB.
- DD: For the univariate histogram density estimator, we use 40 bins and set  $\alpha = 1$ , which corresponds to the pseudo-counts added to each bin.
- Tree: We set the max leaf nodes of the density tree destructor to 10 with a uniform weight of 0.9, which highly regularizes the density estimators. For example, a uniform weight of 1 corresponds to the tree merely being the uniform distribution over the whole unit hypercube.
- SIG: We use the code from original github repo for the SIG paper [Dai and Seljak, 2020]. They recently change some of their code so to show what we actually used, we include the original SIG code file in our code and will only use those codes in this SIG experiment for 2D data ( $k = 2$ ).

##### More than two class distributions ( $k > 2$ )

- Basically the setup is very similar to the  $k = 2$  case. The differences are listed as below.
- Number of layers: All iterative models (including mSWD-NB, NB-mSWD-NB, Rand-NB, NB-Rand-NB, DD, Tree, SIG) use 30 layers.
- Number of dimensions for orthogonal transformation: We apply orthogonal transformation in the space with dimension 2.
- DD: It is basically the same as the  $k = 2$  case but with a different initial destructor. Additionally, we add a normal distribution CDF and inverse CDF as pre and post processing transformations.

#### D.5 Models for MNIST and FashionMNIST

##### Two class distributions ( $k = 2$ )

- Number of dimensions for mSWD-NB: We use orthogonal transformation with  $m = 30$  directions which is much smaller than the ambient dimensions of  $d = 784$  similar to the the SIG paper [Dai and Seljak, 2020].
- Number of layers: We use 250 layers for mSWD-NB and 10 layers for DD. In this way, the product of the number of layers and the number of dimensions while fitting the NB/DD are approximately the same i.e.  $250 \times 30 \approx 10 \times 784$ .

- **mSWD-NB**: We add a normal distribution inverse CDF and CDF at the start and the end of the entire mSWD-NB model as pre and post processing transformations to project the unit data into the real space for transformation.
- **DD**: The setup of DD is basically the same as what we use for 2D experiments with  $k > 2$  except that we remove the pre and post processing transformations with the normal distribution CDF and inverse CDF since the data is already on the unit hypercube.
- **mSWD-Tree**: We use 250 layers. We set the max leaf nodes of the tree destructor to 30 with a uniform weight of 0.5.
- **Tree**: We use 500 layers because we observe that Tree tends to need more layers to get reasonable results. We set the max leaf nodes of the tree destructor to 30 with a uniform weight of 0.1.
- **Alignflow**: The AlignFlow implementation is done through the direct clone from the Github repository with some modifications on the code and parameters setup. We first follow the AlignFlow paper to have these general parameters getting set up: the batch size is 16, the learning rate is set to a fixed  $2e-04$ , maximum gradient norm is 10. We train 50 epochs for choices of the lambda value  $1e-05$  and  $1e-04$ . For the Real-NVP model, the model is a four scale setup. The first three scales contain three checkerboard coupling layers followed by three channelwise coupling layers. Then the data is squeezed and split so that half the data goes to the next scale. For the final scale, we only perform the checkerboard coupling layer four times. The squeeze operation is simply by turning each subvolume  $4 \times 4 \times 1$  into the subvolume  $1 \times 1 \times 4$ . And the splitting operation tries to split the last dimension into two parts. Also within each coupling layer, we parameterize the scale and translate factors by using the ResNet structure with number of blocks equals 4. And the number of channels for the ResNet is set to 32 and gets doubled every time when we switch the coupling layer from checkerboard layer to channelwise layer. For the GAN setup, the discriminator is set to have 5 convolutional layers with kernel size 4 and stride 1. The number of channels is doubled each time when passing to the next layer with the initial value 32 for the generator and 64 for the discriminator.

#### More than two class distributions ( $k = 3$ )

- **GBNB**: We add a GBNB model here as a comparison which is a full-dimensional GB layer followed by a full-dimensional NB layer.
- The setup of other models is exactly the same as the  $k = 2$  case.

#### More than two class distributions ( $k = 10$ )

- **Number of dimensions for mSWD-NB**: We use orthogonal transformation with  $m = 10$  to transform the original distribution with dimension  $d = 784$ .
- **Number of layers**: We use 100 layers for mSWD-NB since the working dimension is only  $m = 10$  for each layer while for DD we only use 10 layers because the working dimension is  $d = 784$ . Thus, if we compare the total number of dimension-wise transformations mSWD-NB has  $100 \times 10 = 1000$  transformations while DD can have  $784 \times 10 = 7840$  transformations. Nevertheless, mSWD-NB still performs better in general based on our quantitative and qualitative results in other sections.

## D.6 Metrics for 2D Experiments

- **Transportation cost** - We find the averaged squared distance for each class separately and use uniform weight to take the average over all class distributions, i.e.,

$$\frac{1}{k} \sum_j \frac{1}{|X_j|} \sum_{x \in X_j} \|x_i - \hat{T}_j(x_i)\|_2^2, \quad (17)$$

where  $|X_j|$  is the number of samples in the test set for the  $j$ -th class distribution and  $\hat{T}_j$  are the estimated maps.

- **Wasserstein distance** - For the test samples, we form “fake” samples for each class distribution by using the estimated maps, i.e.,

$$\tilde{X}_{j' \rightarrow j} = \hat{T}_j^{-1}(\hat{T}_{j'}(X_{j'})), \quad \forall j' \neq j, \quad (18)$$

where  $\hat{T}_j$  are the estimated maps. We then use the Sinkhorn algorithm (with  $\epsilon = 0.1$  and maximum iterations set to 100) to estimate the WD between the real and fake samples over all possible real-fake pairs, i.e.,

$$\frac{1}{k^2 - k} \sum_{j=1}^k \sum_{j' \neq j}^k \text{SinkhornWD}(X_j, \tilde{X}_{j' \rightarrow j}). \quad (19)$$

- **Repetitions** - We repeat the entire map estimation process and metric evaluation 5 times to average over random effects and calculate standard deviations for each method.

## D.7 Metrics for MNIST and FashionMNIST

**Transportation Cost** The setup for transportation cost is the same as 2D experiments except for the experiment with AlignFlow since the scale of the input and output are different in AlignFlow. Specifically, iterative methods such as GB, NB, mSWD-NB, and DD, have images and latent spaces to be in the range  $[0, 1]$  for each dimension. However, in AlignFlow, images are normalized into  $[-1, 1]$ , and the latent space is a normal distribution. Therefore, for the purpose of comparison with all the iterative methods, we need some modifications on the transportation cost for the AlignFlow. We can rescale the input domain from  $[-1, 1]$  to  $[-0.5, 0.5]$  simply by dividing the input by 2, which gives a unit domain as for the iterative methods. We can do the same for the latent space which makes the Gaussian prior to have a standard deviation 0.5 instead of 1. By doing these pre and postprocessing steps, we can get approximately the same scale in both image space and latent space as the unit scale for the iterative methods. The transportation cost is then  $c(\frac{1}{2}x, \frac{1}{2}z) = \|\frac{1}{2}(x - z)\|^2 = \frac{1}{4}c(x, z)$ . Therefore, we manually divide the transportation cost computed in the unscaled space by a factor of 4 for the AlignFlow paper for the purpose of fair comparison. Note that this added scaling favors the baseline method AlignFlow—without it, the AlignFlow transportation cost would be worse. Additionally, because AlignFlow is so computationally expensive, we do not repeat the estimation process five times and thus cannot compute standard deviation for AlignFlow transportation costs.

**Cross Entropy Loss** The new metric here is the cross entropy loss evaluated by CNN classifier to replace WD in the 2D experiments because empirical WD is not close to the population WD in high dimensions [Genevay et al., 2019].

- *Structure of CNN classifier* - We use different classifiers for MNIST and FashionMNIST experiments because FashionMNIST is a harder task for CNN classifier. The MNIST classifier is copied directly from (<https://www.kaggle.com/dsaichand3/mnist-classifier-in-pytorch>). It contains two convolutional layers and two fully connected layers with maxpooling, dropout and ReLUs. The FashionMNIST classifier is directly from (<https://www.kaggle.com/pankajj/fashion-mnist-with-pytorch-93-accuracy>). It contains two convolutional layers and three fully connected layers with maxpooling, dropout, batch norm, and ReLU layers.
- *Parameters of CNN classifier training* - We use 30 epochs with batchsize=64 and lr=1e-4. We use Adam optimizer for both datasets but for MNIST beta1 is set to be 0.5 while for FashionMNIST beta1 is set to be 0.9.
- *Training of CNN classifier* - As stated in the section of Datasets, the datasets are divided into three parts,  $X^{(\text{train})}$ ,  $X^{(\text{cnn})}$ ,  $X^{(\text{eval})}$ .  $X^{(\text{train})}$  is used for optimizing the symmetric Monge map problem.  $X^{(\text{cnn})}$  is used for training the CNN classifier.  $X^{(\text{eval})}$  is used to compute the final cross entropy loss using the trained CNN classifier. For each class distribution, we have real samples and fake samples based on translating from other class distributions, i.e.,  $X_j^{(\text{cnn})}$  are the real samples for the  $j$ -th class distribution and

$$\tilde{X}_j^{(\text{cnn})} = \text{concatenate}(\{\hat{T}_j^{-1}(\hat{T}_{j'}(X_{j'}^{(\text{cnn})}))\}_{j' \neq j}), \quad (20)$$

are the fake samples for the  $j$ -th class distribution generated from the other class distributions by using the estimated symmetric maps  $T_j$ . We subsample  $\tilde{X}_j^{(\text{cnn})}$  to have the same number of samples as  $X_j^{(\text{cnn})}$  and train a CNN classifier for each class distribution, i.e.,  $k$  CNN classifiers are trained that try to distinguish between the real samples ( $X_j^{(\text{cnn})}$ ) and the fake samples ( $\tilde{X}_j^{(\text{cnn})}$ ) of each class distribution.

- *Average test cross entropy loss on  $X^{(\text{eval})}$*  - We then use  $X^{(\text{eval})}$  to create real and fake examples as above for testing and compute the test cross entropy loss using the previously trained CNN classifier. For the iterative methods, we repeat the entire symmetric Monge map estimation, CNN training, and evaluation five times to average over random effects. However, for AlignFlow, because the map estimation is so computationally expensive, we only repeat the CNN training and evaluation five times while keeping the same maps. Finally, we take the average cross entropy loss over all classes and all repetitions as the final measure.

## E ADDITIONAL AND EXPANDED FIGURES

This section includes the qualitative results for additional experiments and expanded figures from the main paper.



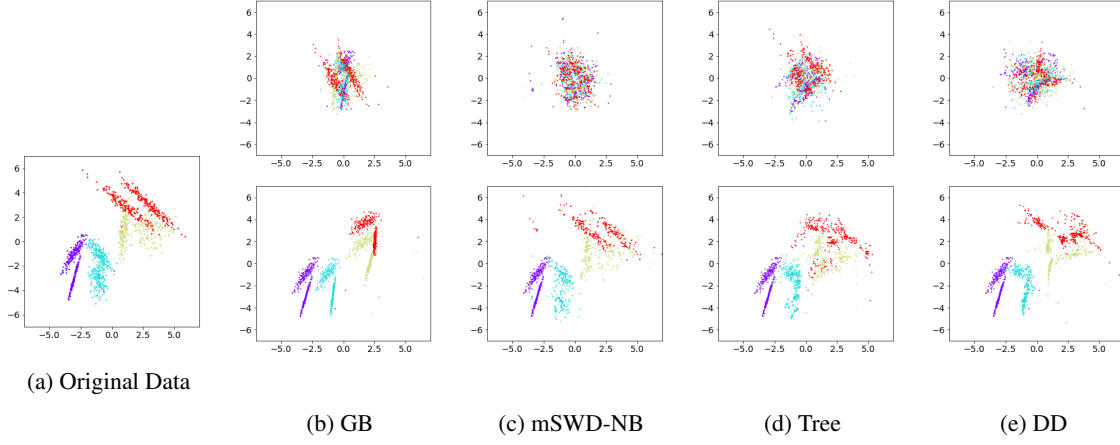


Figure 4: 2D Random Pattern Data ( $k = 4$ ). The top row is latent distribution  $Z_0$  (the latent distribution found by class 0 data). The bottom row is the corresponding flipped distribution from  $Z_0$ .

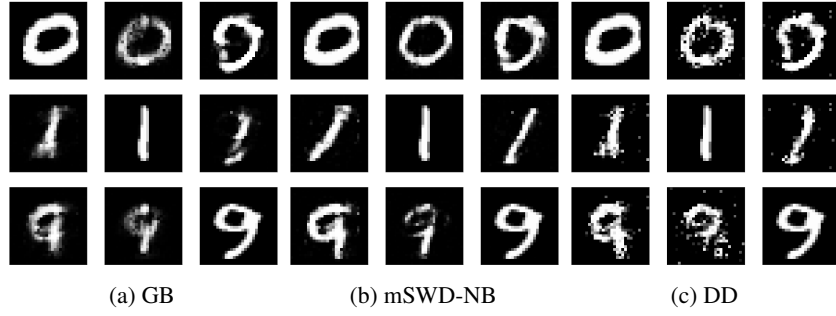


Figure 5: Samples of MNIST ( $k = 3$ ). The diagonal is the real sample and each column represents mappings to the other digits.

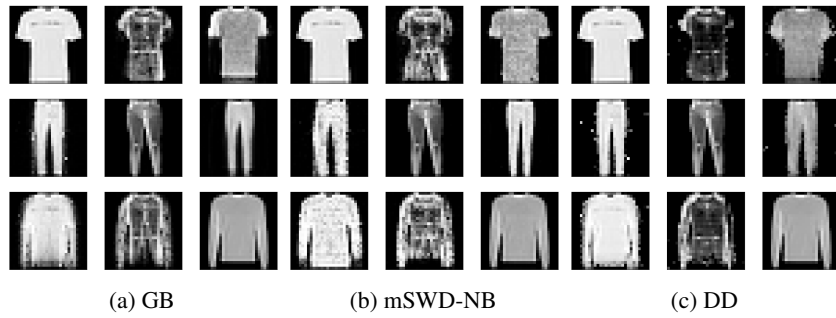


Figure 6: Samples of FashionMNIST ( $k = 3$ ). The diagonal is the real sample and each column represents mappings to the other digits.

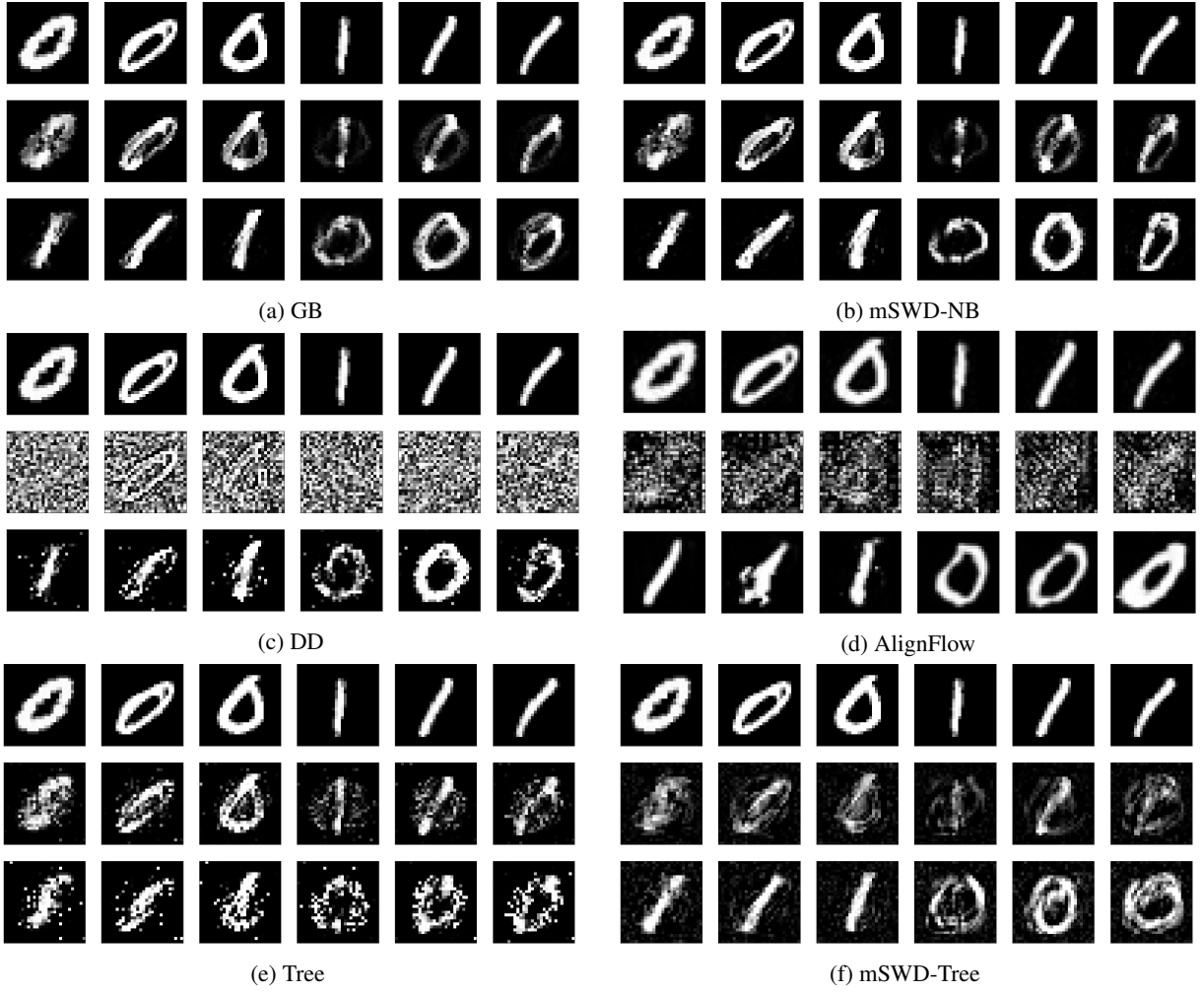


Figure 7: Expanded figure of MNIST ( $k = 2$ ). The first row represents the original samples. The second row represents the latent representation. The third row represents the flipped samples.

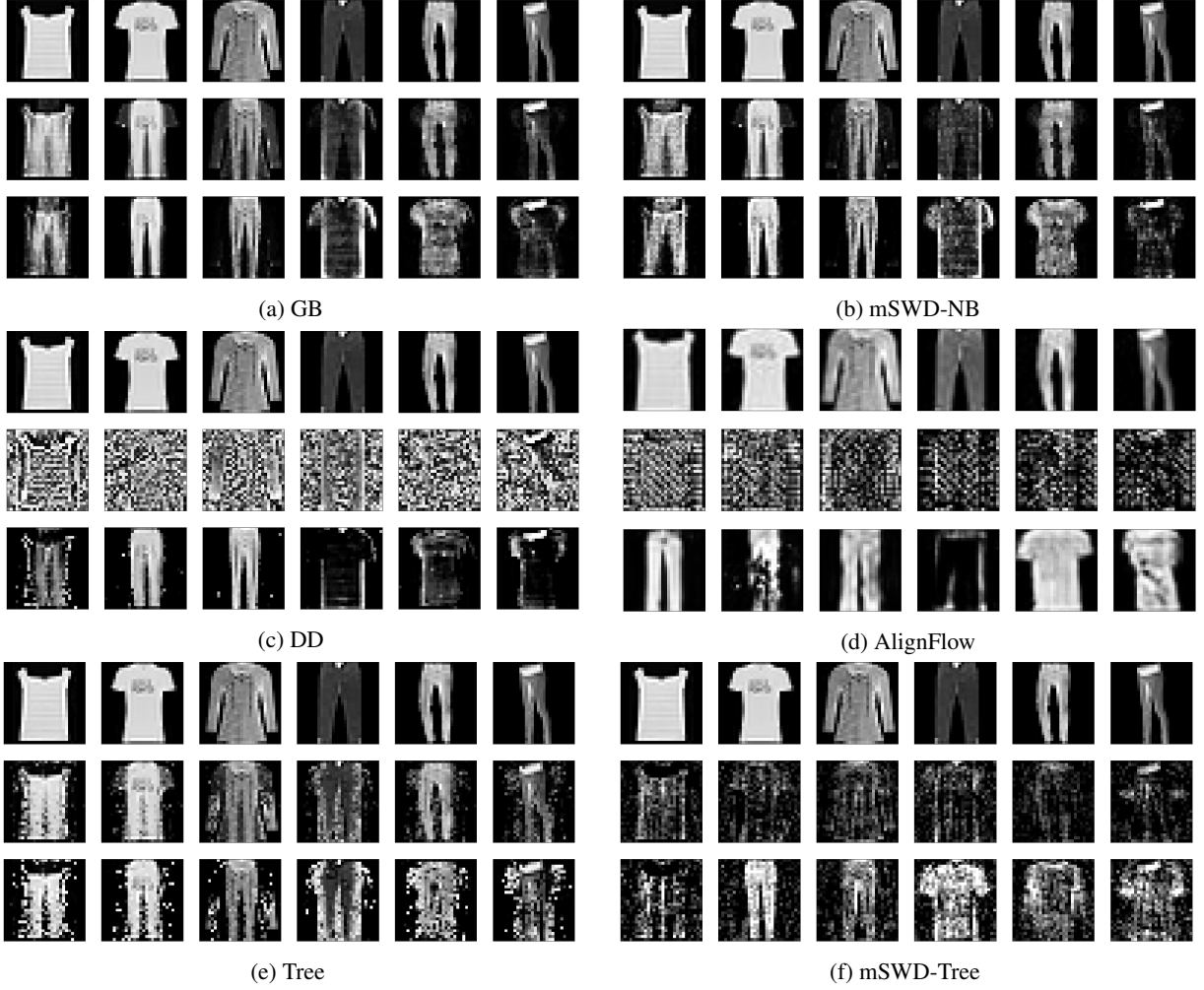
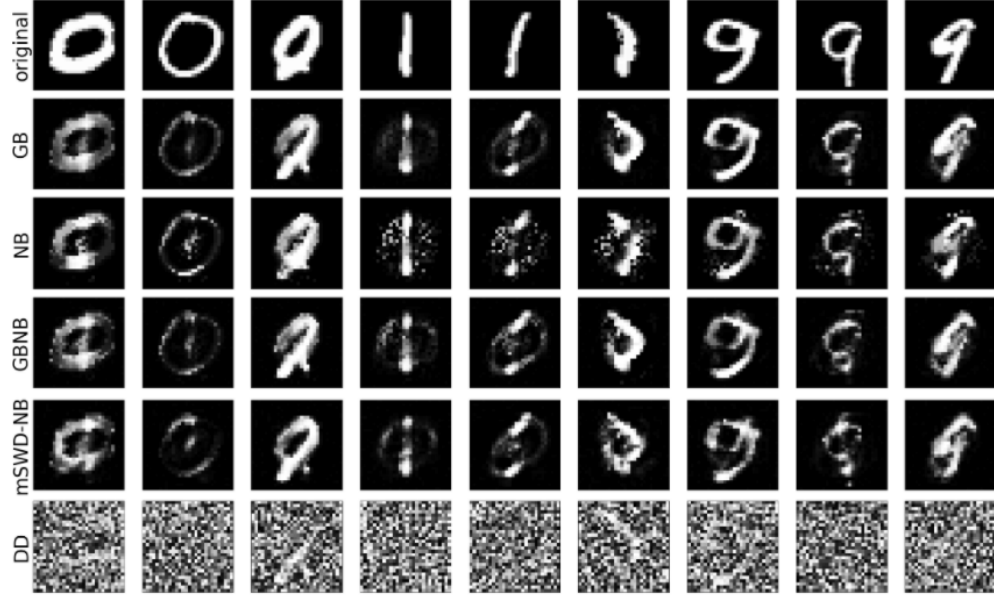
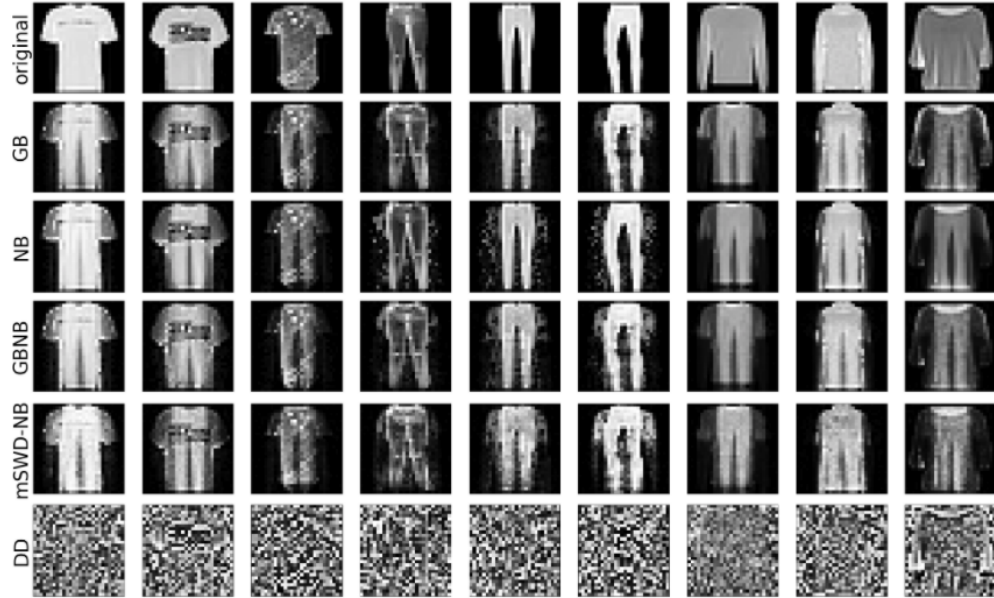
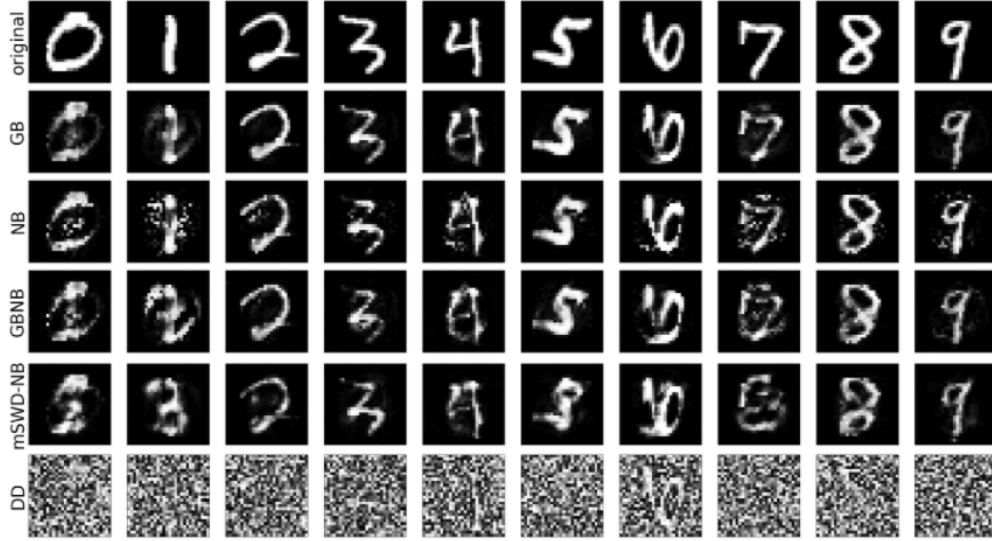
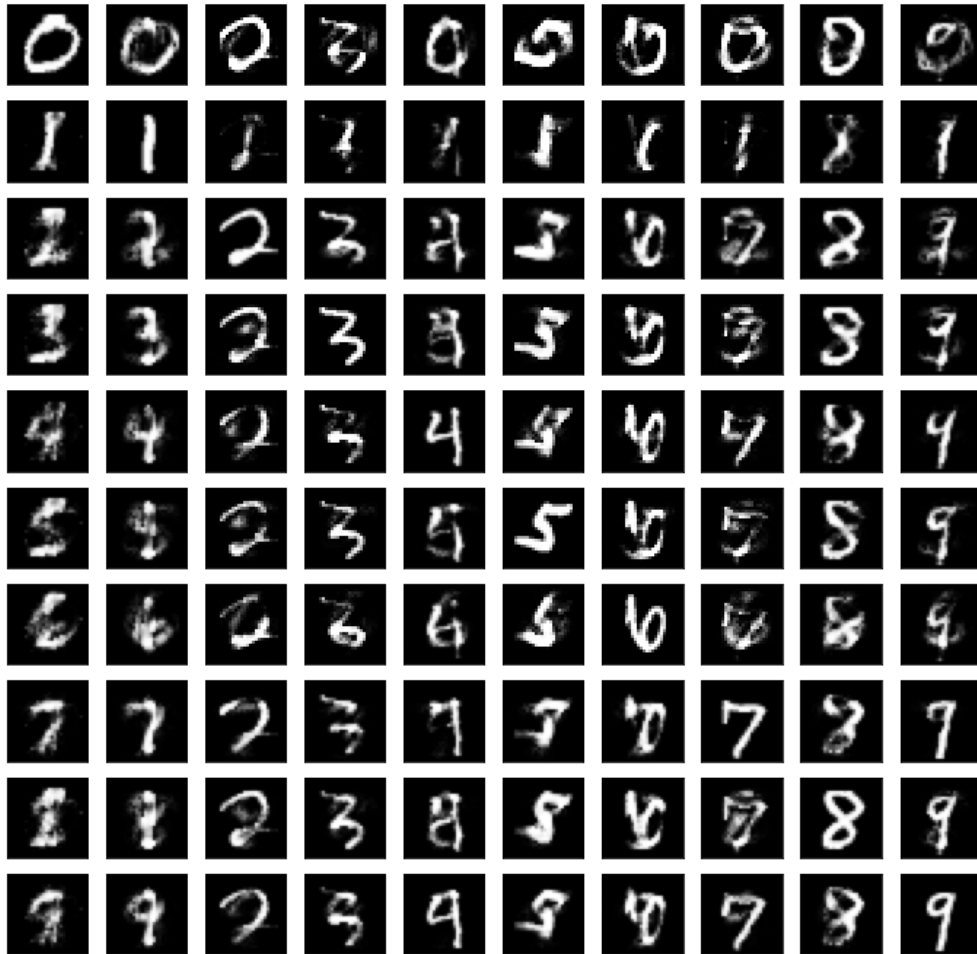


Figure 8: Expanded figure of FashionMNIST ( $k = 2$ ). The first row represents the original samples. The second row represents the latent representation. The third row represents the flipped samples.

Figure 9: More latent representation examples for MNIST ( $k = 3$ ).Figure 10: More latent representation examples for FashionMNIST ( $k = 3$ ).

Figure 11: Latent representation of MNIST samples ( $k = 10$ ).Figure 12: Multi-domain ( $k = 10$ ) results for MNIST with GB. The diagonal is the real sample and each column represents mappings to the other digits.

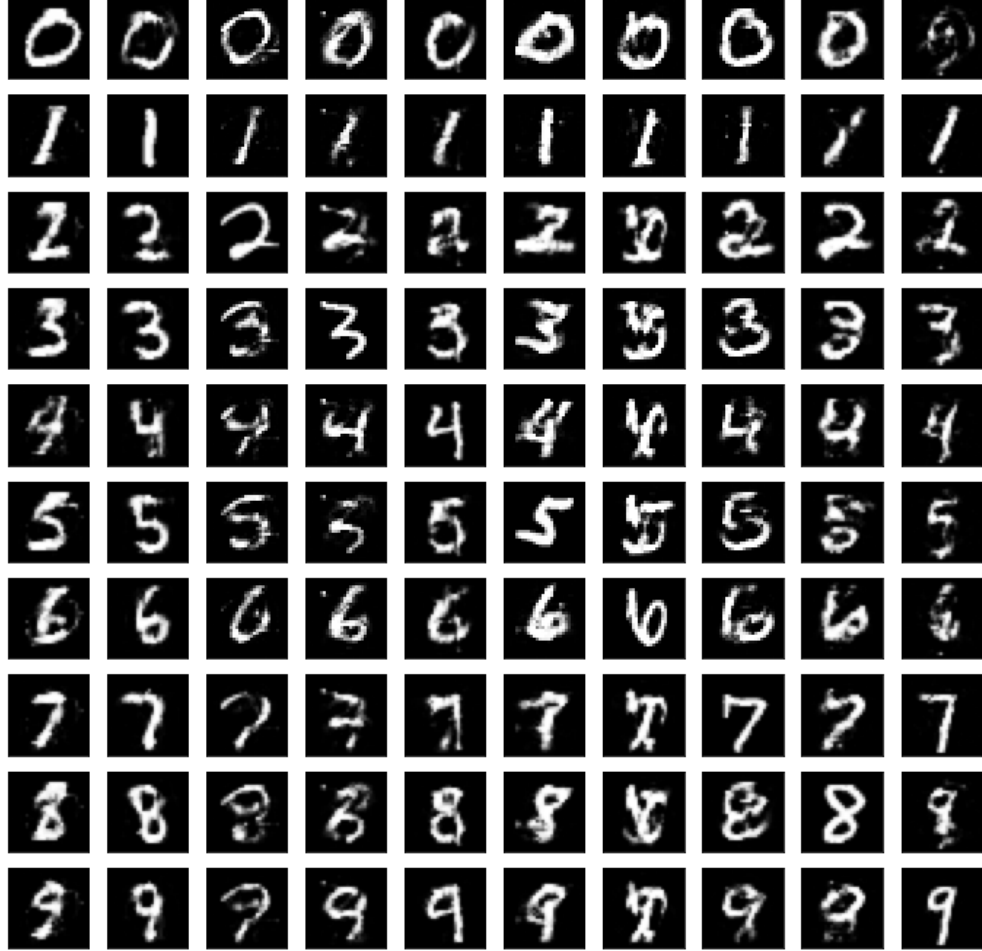


Figure 13: Multi-domain ( $k = 10$ ) results for MNIST with mSWD-NB. The diagonal is the real sample and each column represents mappings to the other digits.

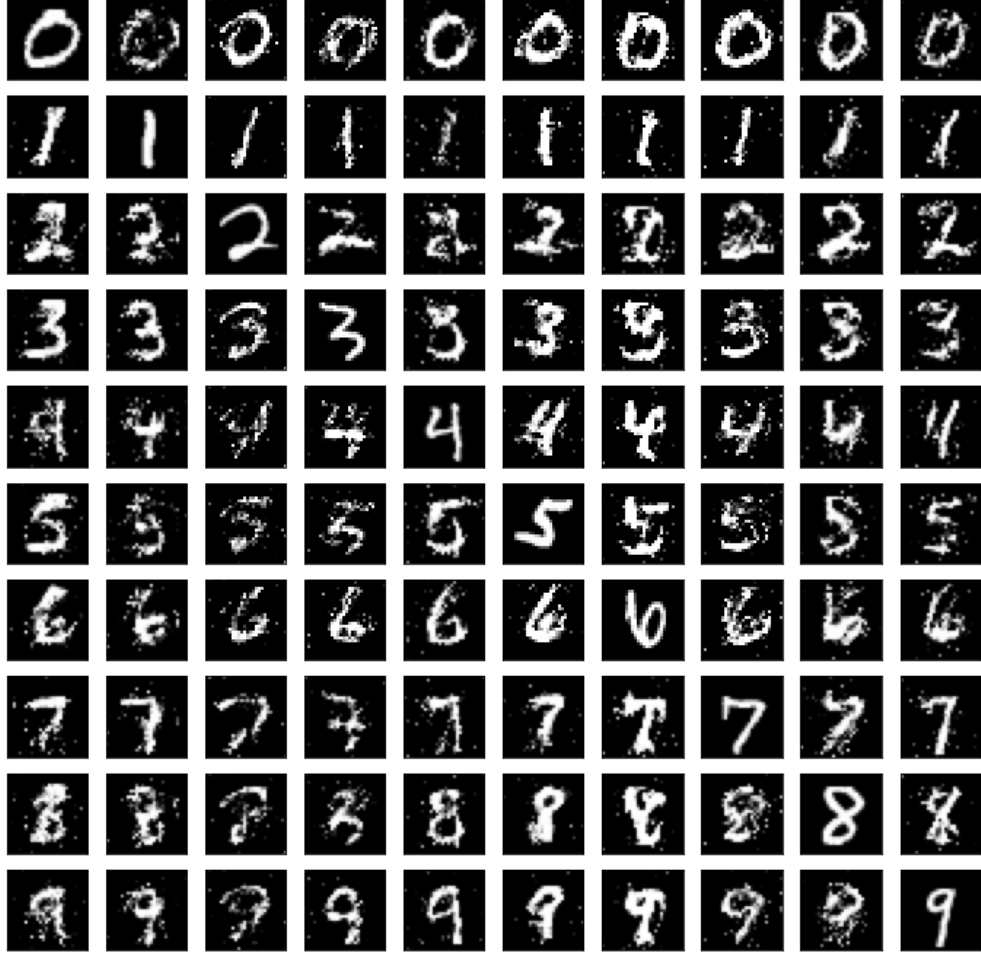


Figure 14: Multi-domain ( $k = 10$ ) results for MNIST with DD. The diagonal is the real sample and each column represents mappings to the other digits.

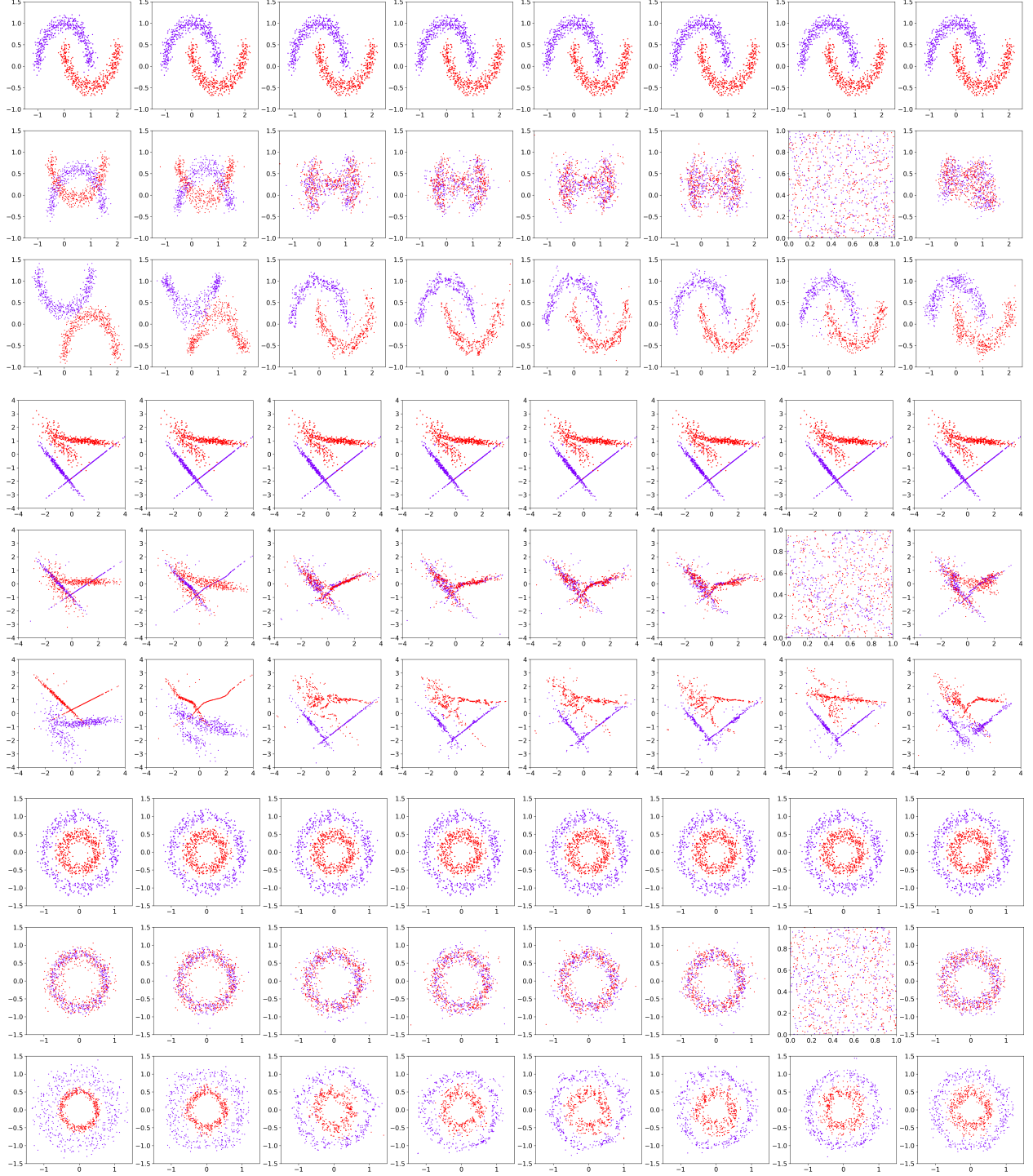


Figure 15: Expanded figure of 2D Data ( $k = 2$ ). In each sub figure, the first row represents the original data. The second row represents the latent distribution. The third row represents the flipped distribution. The columns from left to right represent the model: GB, NB, mSWD-NB, NB-mSWD-NB, Rand-NB, NB-Rand-NB, DD, Tree.



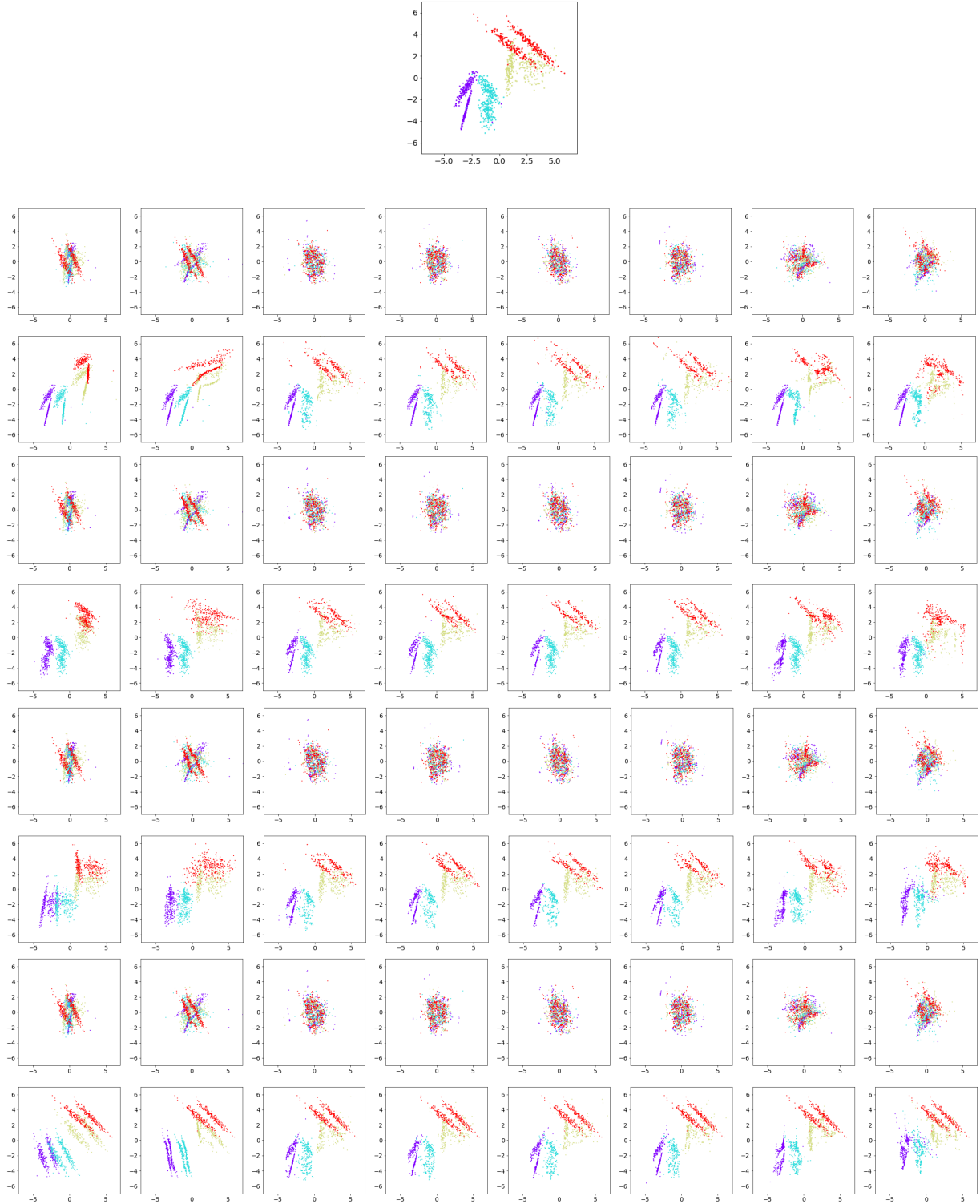


Figure 16: Expanded figure of 2D Random Pattern ( $k = 4$ ). The columns from left to right represent the model: GB, NB, mSWD-NB, NB-mSWD-NB, Rand-NB, NB-Rand-NB, DD, Tree. The top image is the original distribution. Each pair of rows represents the translation of samples from one class distribution to all other class distributions. We can translate every class distribution to every other class distribution since all functions are invertible. The pairs of rows are the results of translating from different source distributions, i.e., class 1 (purple), class 2 (turquoise), class 3 (yellow), and class 4 (red) distributions respectively. The top of each pair is the shared latent representation (the same across all rows) whereas the bottom row shows the generated data. Note that if the source and target distribution are the same, e.g., from class 1 to class 1, the output distribution will be exactly as in the original since our transformations are invertible.

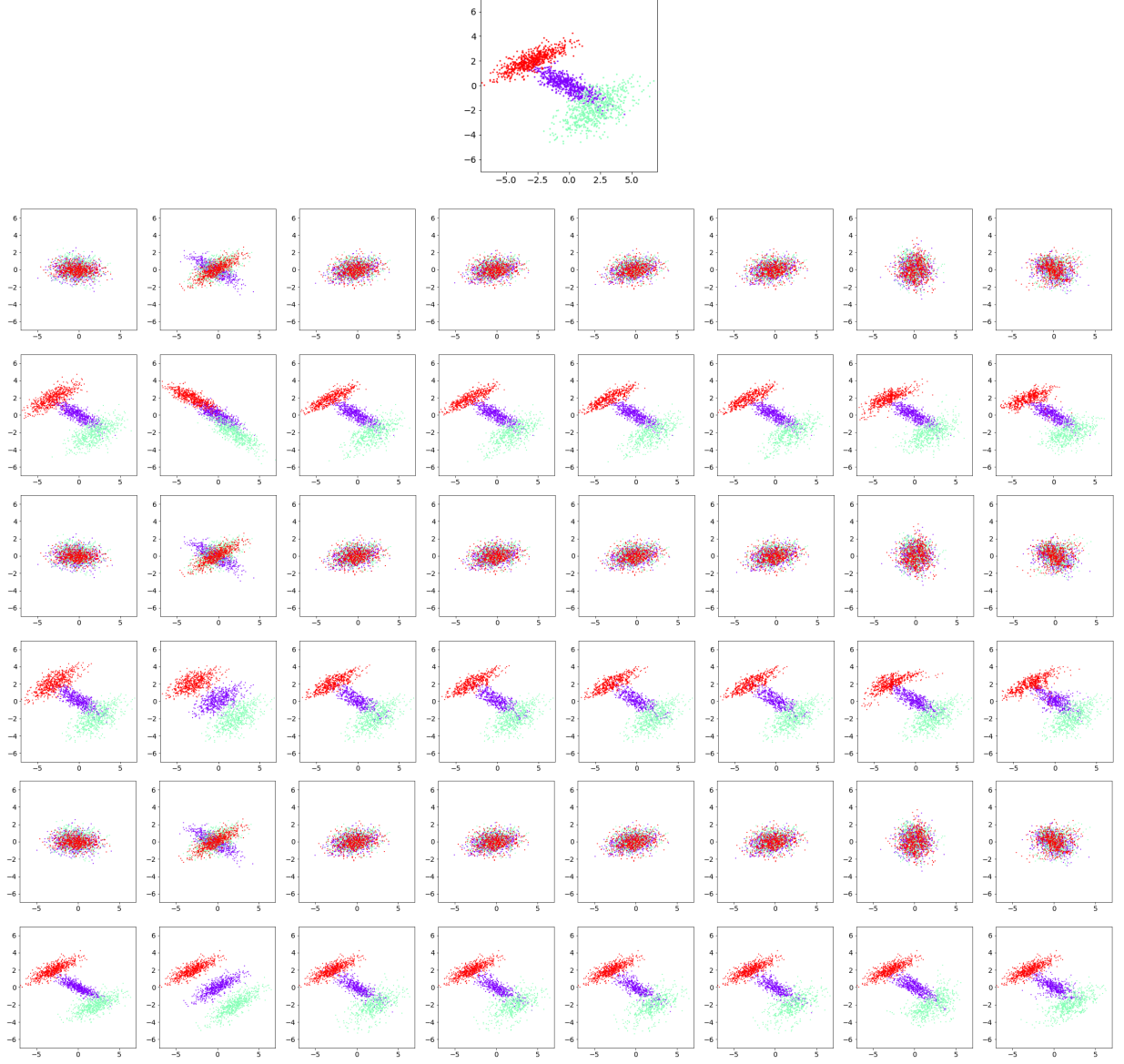


Figure 17: Expanded figure of 2D Gaussian ( $k = 3$ ). The columns from left to right represent the model: GB, NB, mSWD-NB, NB-mSWD-NB, Rand-NB, NB-Rand-NB, DD, Tree. The top image is the original distribution. See caption of Fig. 16 for explanation of each pair of rows.